THESIS FOR THE DEGREE OF DOCTOR OF PHILOSOPHY

Antibacterial Surfaces for Biomedical Applications

SABA ATEFYEKTA

Department of Chemistry and Chemical Engineering

CHALMERS UNIVERSITY OF TECHNOLOGY

Gothenburg, Sweden 2020

Antibacterial surfaces for biomedical applications

SABA ATEFYEKTA
ISBN 978-91-7905-228-7

Doktorsavhandlingar vid Chalmers tekniska högskola
Ny serie nr 4695
ISSN 0346-718X

Department of Chemistry and Chemical Engineering
Chalmers University of Technology
SE-412 96 Gothenburg
Sweden
Telephone + 46 (0)31-772 1000

Cover:
SEM image of *staphylococcus epidermidis* biofilm grown on an Elastin-like polypeptide coated titanium disk.

Printed by:
Chalmers Reproservice
Gothenburg, Sweden 2020

“Our virtues and our failures are inseparable, like force and matter. When they separate, man is no more.”

- Nicola Tesla

Antibacterial surfaces for biomedical applications

SABA ATEFYEKTA
Department of Chemistry and Chemical Engineering
CHALMERS UNIVERSITY OF TECHNOLOGY

ABSTRACT

Medical devices such as orthopedic implants are intended to serve for improved quality of life. However, clinical success cannot be taken for granted and the most common reason for failure is due to biomaterials associated infection (BAI). An implantation surgical site is a susceptible environment for bacterial colonization, which in combination with compromised immune system, results in that bacteria can develop biofilms on the implant surface or in adjacent tissue. Once such a biofilm has established, it may lead to an infection that cannot be eradicated by means of traditional antibiotics, often resulting in revision surgery. Wounds after post implantation surgery is another risk for bacterial colonization into underlying tissue and increases further the susceptibility to infection. These and other bacteria related complications are today becoming more serious due to the rapid increase of antibiotic resistance worldwide. This has resulted in that many available antibiotics are losing their potency against bacteria and consequently, treating an infection with antibiotics is not working as effectively as in the past.

The objective of this thesis was to find new solutions to address the complications associated with bacterial colonization through applying preventive measures by designing antibacterial surfaces for inhibition of early biomaterials associated and wound infection. For this purpose, two types of antibacterial surfaces were designed and evaluated. In the first type, a local drug-delivery system based on mesoporous titania thin film was developed. This film was to serve as implant coating where antibiotics are released locally at the implantation site to prevent biofilm formation and subsequent tissue colonization. In the second approach, antibacterial surfaces were developed through covalent immobilization of a cationic antimicrobial peptide (AMP), thus creating surfaces that kill bacteria upon contact.

The overall results in this thesis, which are presented as four papers, suggest that the developed antibacterial surfaces are promising to use in future biomedical applications.

Keywords: Antibacterial surfaces, antibiotic delivery, contact killing surfaces, mesoporous titania, antimicrobial peptides, infection, elastin-like polypeptides, implants, medical devices.

LIST OF PUBLICATIONS

I. Antimicrobial performance of mesoporous titania thin films:
role of pore size, hydrophobicity and antibiotic release
Saba Atefyekta, Batur Ercan, Johan Karlsson, Erik Taylor, Stanley Chung, Thomas J Webster and Martin Andersson
Int. J. Nano Med. 2016, 11; 977–990

II. Development of a photon induced drug-delivery implant coating
Ali Alenezi, Mats Hulander, Saba Atefyekta and Martin Andersson
Mater. Sci. Eng. 2019, 98; 619-627

III. Antibacterial elastin-like polypeptides coatings: functionality stability, and selectivity
Saba Atefyekta, Maria Pihl, Chris Lindsay, Sarah C.Heilshorn and Martin Andersson
Acta Biomater. 2019, 83; 245-256

IV. Antibacterial hydrogels for prevention of wound infection
Saba Atefyekta, Edvin Blomstrand, Anand Kumar Rajasekharan, Jaan Hong, Sara Svensson, Thomas J Webster, Peter Thomsen and Martin Andersson
Manuscript for submission

CONTRIBUTION REPORT TO THE LISTED PUBLICATIONS

I. Performed all experimental work and wrote the manuscript. Parts of the experiments were performed in collaboration with Thomas Webster nanomedicine lab at Northeastern University, Boston, USA.

II. Performed the experiments for preparation of mesoporous titania coatings, antibiotic loading and bacteria assays. Wrote part of the manuscript.

III. Performed all experimental work including elastin-like protein expression and purification and wrote the manuscript. Parts of the experiments were performed in collaboration with Sarah Heilshorn's lab at Stanford University, CA, USA.

IV. Performed all experimental work except MTT assays, MRSA assays and animal surgery procedure and wrote the manuscript.

PUBLICATIONS NOT INCLUDED IN THIS THESIS

1. Controlling drug delivery kinetics from mesoporous titania thin films by pore size and surface energy
   Johan Karlsson, Saba Atefyekta and Martin Andersson
   Int. J. Nano Med., 2015, 10; 4425–4436

2. Modulation of nanometer pore size improves magnesium adsorption into mesoporous titania coatings and promotes bone morphogenic protein 4 expression in adhering osteoblasts
   Francesca Cecchinato, Saba Atefyekta, Ann Wennerberg, Martin Andersson, Ryo Jimbo, Julia R Davies
   Dental Mater., 2016, 32 (7); 148-158

3. Stem cell homing using local delivery of plerixafor and stromal derived growth factor-1alpha for improved bone regeneration around Ti-implants
   Johan Karlsson, Necati Harmankaya, Anders Palmquist, Saba Atefyekta, Omar Omar, Pentti Tengvall and Martin Andersson
   J. Biomed. Mater. Res. A, 2016, 104 (10); 2466-2475

4. Osseointegration effects of local release of strontium ranelate from implant surfaces in rats.
   Ali Alenezi, Silvia Galli, Saba Atefyekta, Martin Andersson, Ann Wennerberg
   J. Mat. Sci. Materials in Medicine. 2019, 30 (10); 116

TABLE OF CONTENTS

ABBREVIATIONS

AMP	Antimicrobial peptide
ALP	Alkaline Phosphatase
BAI	Biomaterial associated infection
DCDMS	Dichlorodimethylsilane
EDC	1-ethyl-3-(3-dimethylaminopropyl) carbodiimide hydrochloride
EISA	Evaporation induced self-assembly
ELP	Elastin-like polypeptide
GNRs	Gold nanorods
hMSCs	Human bone marrow-derived mesenchymal stem cells
LLC	Lyotropic liquid crystal
MPT	Mesoporous titania
NHS	*N*-Hydroxysuccinimide
PNIPAAM	Poly(N-isopropylacrylamide)
QCM-D	Quartz crystal microbalance with dissipation monitoring

1 *A big problem*

"If we don't act now, our medicine cabinet will be empty, and we won't have the antibiotics we need to save lives."

Center for disease control (CDC) Director, Tom Frieden

What does a world without antibiotics mean to us? Can we imagine a world where many millions of women dying in child birth, impossible chemotherapy treatments for cancer patients, no organ transplant, no routine surgeries and small wounds turning into life threatening conditions?

Today, we are standing on the edge of a post-antibiotic era, a dreadful scenario where antibiotics are not efficient anymore and simple infections can become mortal. Although the seriousness of the antibiotic resistance problem is pointed out repeatedly by international public health institutes such as World Health Organization (WHO), there is still a constant tension between the necessity of using antibiotics to cure an infection and the adverse outcome of their use which is developing resistance by bacteria. Antibiotic resistance occurs when bacteria that are exposed to antibiotics, in an evolutionary process, develop genes encoding resistance and pass them along to create a full generation of resistant microbes. This problem is progressing so rapidly that UN has called it a "global health emergency". In order to fight the war against antibiotic resistance, we need immediate actions. Antibiotic resistance should be stopped before it becomes a real crisis and before a big population gets affected.

Believing that one of the most effective ways to reduce antibiotic resistance is a reduction in the use of antibiotics lies behind the motivation of this thesis, that is, to introduce new solutions to stop or decrease unnecessary usage of antibiotics linked to implant surgeries or wound management routines.

2 Introduction

"Good health is a temporary condition" as physiatrists say. Although natural healing processes and defense immune system helps the human body to heal from a variety of illnesses and injuries by its own, at some point, it will face serious health conditions that need advanced healthcare solutions to help its healing process along. For instance, over the past decades the demand for medical implants and devices has considerably increased in order to help restore organ failures that arise from chronic diseases, aging population and traumas.[1] However, one major complexity of using medical implants, is the elevated risk of infection.[2] Bacterial colonization of biomaterial surfaces and surrounding tissues in combination with a comprised immune system, undermines the intended performance of biomaterials.[3,4] In addition, most surgical procedures that are performed to insert implants leave a surgical wound. A wound itself creates a susceptible environment for bacterial growth into the damaged skin to generate an infection progressing into underlying tissue.[5] Today, infections cannot as simple as before be treated and eradicated by traditional antibiotic therapy. Patients may endure long-term unsuccessful antibiotic therapy sessions and its subsequent systemic side effects result in long hospitalization and high cost for healthcare systems.[6,7] One reason that complicates the infection control associated with biomaterials and chronic wounds is that up to 80% of human bacterial infections are biofilm associated and bacteria in biofilm community can escape diagnostic procedures, host immune defense and antibiotic therapy.[8] Furthermore, the emergence of antibiotic resistance is happening worldwide, and the world is entering a post-antibiotic era where even simple skin infections can become life-threatening. The potency of available antibiotics is becoming limited since resistant bacteria no longer respond to many available antibiotics.[9,10]

For medical devices to improve the quality of human life, and not to expose additional complexities to it, the most important step would be to avoid bacterial colonization as the first line of defense against infection.[11] Adherent bacteria biofilm on a biomaterial surface, is a potential source of an infection spreading to surrounding tissue. Due to impairment of the host immune response, bacteria can also reside within host cells around the implant and cause recurrent infections.[4] Prevention of biofilm formation and tissue colonization is therefore the main rationale behind extensive efforts in designing and fabricating new generations of antibacterial surfaces.[12]

3 *Objectives*

The main objective of this thesis was to apply preventive strategies in the design of antibacterial surfaces for prevention of early biomaterials associated infections and bacterial colonization at the wound site. For this purpose, two main types of antibacterial surfaces were designed and discussed as shown in Figure 1.

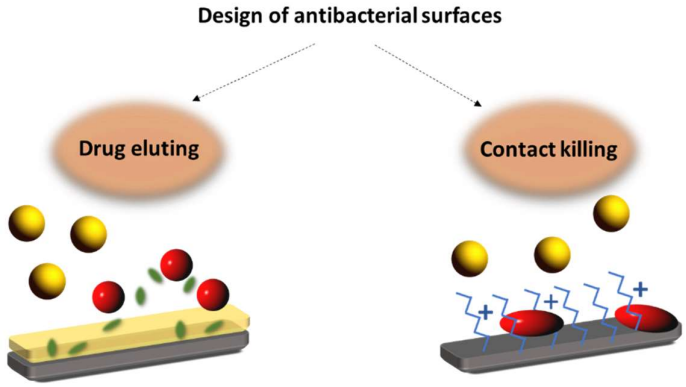

Figure 1. Schematic demonstrating the two types of antibacterial surfaces discussed in this thesis.

The goal of the first approach was to create local drug-delivery systems as implant coatings to release antibiotics directly at the implantation site and prevent biofilm formation and subsequent tissue colonization.

Paper I and II, each introduce a separate drug-delivery model using mesoporous titania (MPT) thin films as antibiotic carriers (Figure 2). Antibacterial performance of MPT thin films with variable pore sizes (2-7nm) and their antibiotic loading and release efficacies, driven by solvent diffusion, are evaluated in paper I, Figure 2a. While in paper II, MPT is used in a combination with a thermoresponsive polymer, PNIPAAm, with incorporated nanorods. This combination is designed to create a photon induced controlled release system, Figure 2b.

Designing contact killing surfaces, is a second approach presented in this thesis. In this strategy, surfaces are modified with covalent immobilization of a cationic antimicrobial peptide (AMP), RRPRPRPRPWWWW-NH_2, to create surfaces that kill bacteria upon contact, Figure 3.

In paper III and IV, two substrates for AMP immobilization are introduced. Recombinantly synthesized elastin-like polypeptides with cell-adhesive RGD motives were used to combine favorable cell properties with antibacterial activities with the aim to create implant coatings that enhance tissue integration and prevent biofilm formation. (Figure 3a). A nanostructured crosslinked lyotropic liquid crystalline hydrogel made of modified pluronic™ F127 (MF127) polymer was applied as a second substrate. Unlike ELP surfaces, MF127 hydrogels do not have cell adhesive sites in their structure. Moreover, the amphiphilic nature of such materials is speculated to favor attachments of AMPs that are amphiphilic molecules as well. Combined with high fluid absorption properties, AMP modification on such substrates can create contact killing surfaces suitable for applications such as wound care patches for prevention of wound associated infections (Figure 3b).

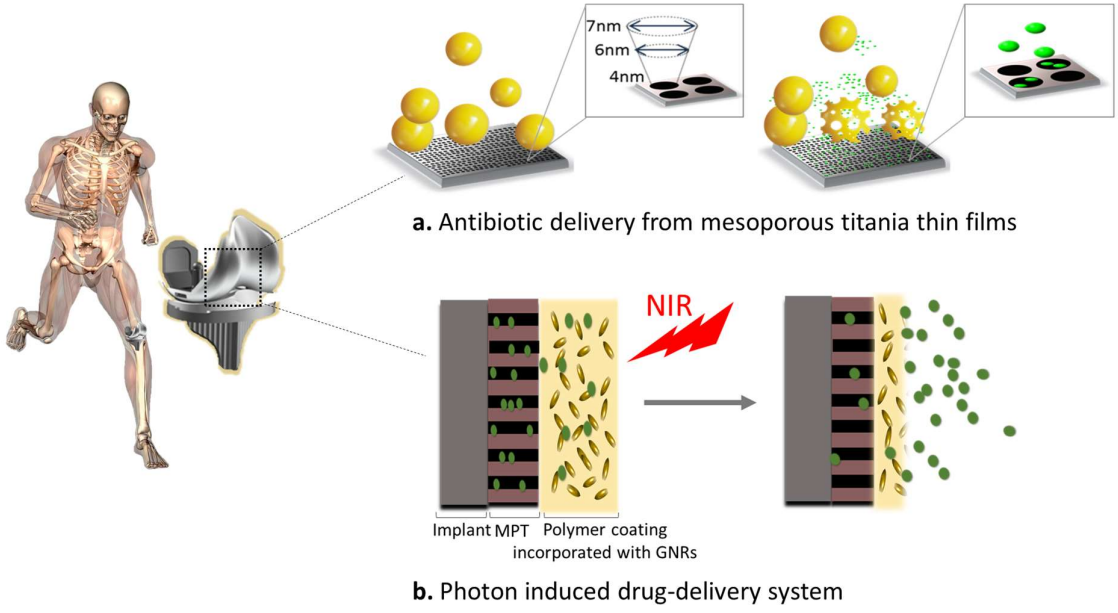

Figure 2. A schematic of the drug-delivery surfaces used in this thesis. **a,** Mesoporous titania thin films with variable pore sizes used for antibiotic delivery and **b,** Mesoporous titania thin films combined with PNIPAAm polymer coating with incorporated nanorods.
MPT=mesoporous titania and GNR= gold nanorods

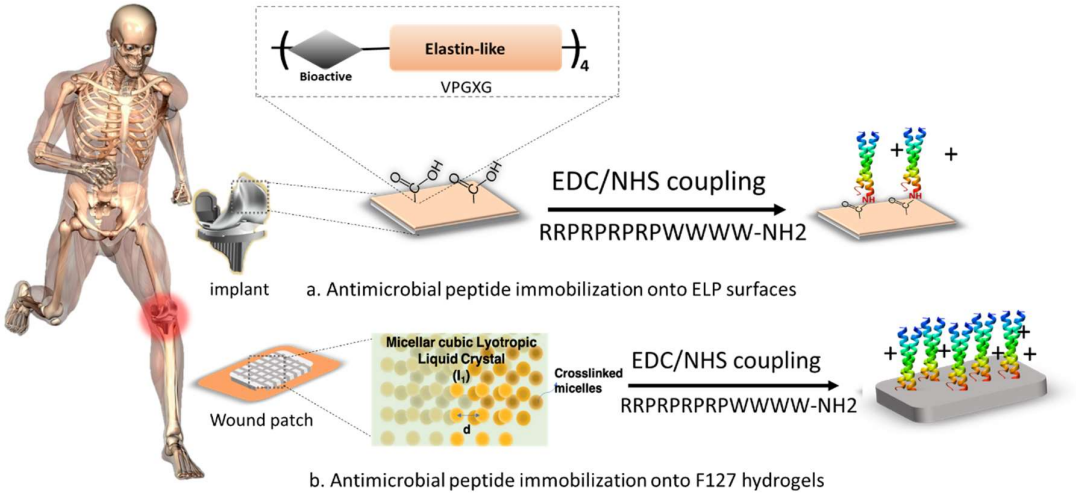

Figure 3. A schematic of the contact killing substrates used in this thesis. **a,** AMP immobilization onto recombinant elastin-like polypeptides with RGD sequences and **b,** AMP immobilization onto cross-linked nanostructured F127 hydrogels.

4 *Background*

To provide a more detailed understanding of the choice of materials and design methods used in this thesis, a background including two main chapters is presented. Chapter 4.1 introduces drug-eluting implant coatings and use of mesoporous titania as antibiotic carriers while chapter 4.2 focuses on contact-killing surfaces using antimicrobial peptides for biomedical applications such as implant coatings and wound care patches.

4.1 Antibiotic eluting surfaces

4.1.1 Local antibiotic delivery

Applying surface coatings that release antibiotics from biomaterials is considered an effective strategy to prevent BAI.[13] Local antibiotic delivery systems introduce an inbuilt functionality to obtain targeted and/or controlled release of antibiotics from biomaterials for prevention of infection.[14] Local administration of antibiotics that can release the drug directly to the site of implantation without the patient having to take systemic doses is a common way to decrease the side effects and drug toxicity while maximizing the treatment outcome.[15] Moreover, a rapid initial release of antibiotics from implant surfaces can be an effective way to prevent the spread of bacteria from surfaces to the surrounding tissue.[4] However, local antibiotic delivery approaches face challenges such as difficulties in controlling the release kinetics with a risk of diluting the antibiotic to a concentration below the minimum inhibitory concentration (MIC) which makes the treatment ineffective. Most importantly, the duration of drug release must be restricted to a limited time period to prevent development of antibiotic resistance.[16] Collectively, such complexities necessitate a careful and practical design of carriers for local antimicrobial drug-delivery systems. Recently, the development of nanomaterials has generated significant advances in improving local antimicrobial drug-delivery systems.[14] For example, mesoporous materials have been highlighted within nanomedicine as a promising drug-delivery system for their unique characteristics, such as high specific surface area and tunable pore size.[17,18]

4.1.2 Mesoporous titania

Over the past decades, the use of mesoporous titania (MPT) has become attractive in various application fields including optics, environmental energy systems, electronics, medicines and biomaterials.[19,20] High surface area, tunable pore size (2-50 nm) and morphology as well as being environmentally friendly and biocompatible are favorable properties of MPT for their growing applications as carriers for sustained drug-delivery and substrates for cell behavior control.[21] The use of mesoporous titania has been highlighted in previous studies as bone anchoring implants to improve apatite formation and subsequent bone bonding[22] as well as improved osseointegration using local delivery of osteoporosis drugs *in vivo*.[23] Moreover, it has been shown that drug loading capacity and release from MPT thin films can be highly influenced by altered pore diameter and surface functionalization.[24] Considering these properties, MPT thin films can be suitable candidates for antibiotic delivery to create antibacterial surfaces, and a sustained release of cephalothin and amoxicillin from MPT coated implants have previously been reported.[25,26] In this thesis, MPT thin films with variable pore sizes, synthesized by evaporation-induced self-assembly (EISA) method, have been evaluated and assessed as carriers for local-delivery of antibiotics such as Gentamicin, Vancomycin and Daptomycin, as shown in Figure 4 (paper I). Additionally, the effect of MPT pore size and hydrophobicity without the use of antibiotic on bacterial attachment was investigated.

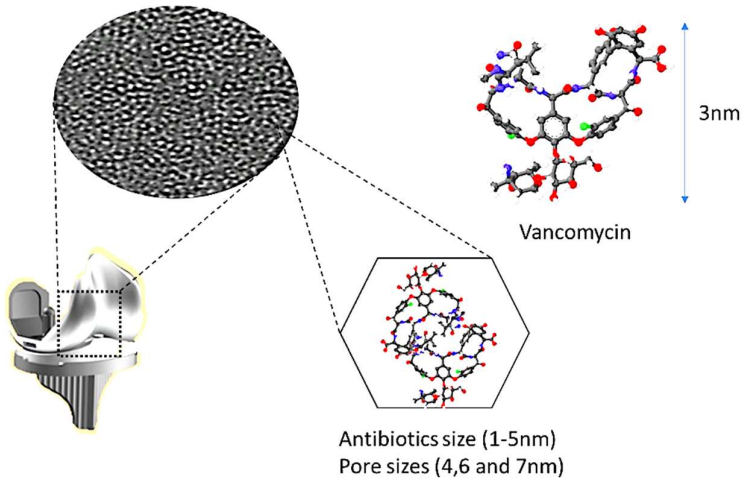

Figure 4. Schematic of antibiotic loading inside mesoporous titania thin films.

4.1.3 Polymer PNIPAAm and GNRs

Introducing polymers for local drug-delivery systems is useful for incorporation of large amounts of drugs as well as to build up a barrier for prevention of undesired too high burst drug release.[27] Introducing a polymer layer around a drug carrier, can help controlling and sustaining the release of drugs into the surrounding media. Among various types of polymers used for this purpose, some polymers show dramatic physical changes upon external stimuli, such as light, pH and temperature.[28,29] Such properties are attractive for designing controlled drug-delivery systems based on polymer response to external factors. For example, the polymer used for designing a drug-eluting implant coating, which is introduced in paper II of this thesis, is a thermo-responsive polymer, poly(N-isopropylacrylamide) (PNIPAAm). This polymer undergoes a phase transition from a swollen hydrophilic state to a shrunken hydrophobic state in response to an increase in temperature (Figure 5).[30,31]

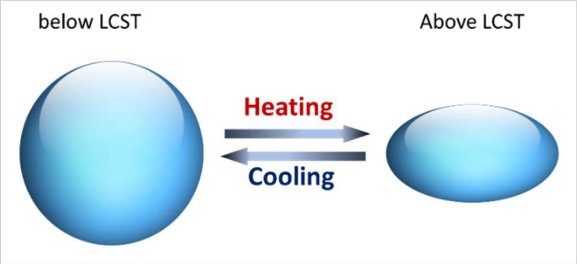

Figure 5. A schematic of volume phase transition of PNIPAAm from a swollen hydrophilic state to a shrunken hydrophobic state below and above the lower critical solution temperature (LCST)

A thin layer of PNIPAAm coating onto drug-loaded MPT thin films can function as a pump that can affect the drug release using a local heating source to control the release from MPT implant coatings. Incorporation of gold nanorods into the polymer, is a suggested strategy to absorb light in the near infrared (NIR) and create heat.[32–35] With this approach, irradiation with NIR can be used as external stimuli to generate heat and create physical change in the polymer structure followed by a sustained drug release from MPT thin films (Figure 6). Several studies have highlighted the successful performance of gold nanorod incorporated PNIPAAm (PNIPAAm-GNRs) upon NIR irradiation.[36,37]

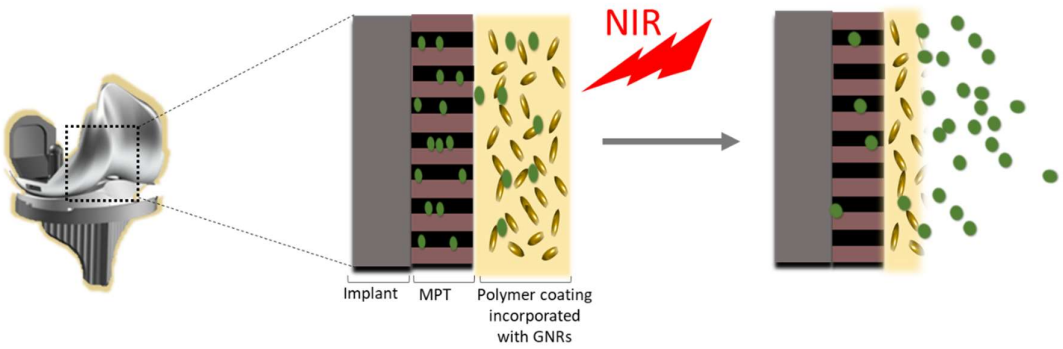

Figure 6. Schematic illustration of a local drug-delivery system as an implant coating, using MPT thin films and PNIPAAm-GNRs.

4.2 Contact killing surfaces

4.2.1 Contact killing

Surfaces can be modified by fixing certain biocides onto them to act on bacterial cells through direct physical contact between the substrate and bacterial membrane. Generally, such surfaces are created by attachment of biocides onto substrates through chemical immobilization.[38] Active surfaces do not contribute as much to bacterial resistance compared to leaching approaches, since they mostly act by causing physical damage to bacterial cells instead of acting on a specific target. Such surfaces do not leach biocides into the surrounding and thus do not impose negative impact on the local environment.[39] Moreover, they usually show broad-spectrum antibacterial activity and are attractive for prevention of bacterial contamination on artificial surfaces. So far, the most studied contact-active biocides are quaternary ammonium compounds and N-chloramines.[40] Creating a surface with a high positive charge density is the main property of such contact killing surfaces that define their antibacterial efficacy.[41]

4.2.2 Antimicrobial peptides

In 1939 the very first antimicrobial peptide (AMP) was discovered in an extract from a soil bacteria (*bacillus*) strain and was shown to protect mice from pneumococci infection[42] In the following years, various types of AMPs have been discovered and found effective against several pathogenic bacteria.[43] The first animal-derived AMP (Defesnin), isolated from rabbit leukocytes, was discovered in 1956 and today, thousands of AMPs have been discovered and synthesized.[44] Antimicrobial peptides are considered the first defense response towards invading pathogens and is present in all classes of life as an important component of the innate immune system.[42,45] In addition, AMPs have also been found to play an important role in regulating inflammatory responses during an infection.[46,47]

As the increasing rate of antibiotic resistant microorganisms limits the use of conventional antibiotics to treat infections, cationic AMPs have received increased attention as a potential alternative.[48,49] Such AMPs have generally an amphiphilic structure consisting of <45 amino acids. The main mode of AMPs mechanism of action involves direct contact with the bacterial surface leading to physical rupturing and breakdown of the cell (Figure 7). The amphiphilic structure of AMPs facilitates their binding to both hydrophilic regions (phospholipid head-groups) and hydrophobic regions (lipid tail-groups) of the bacterial membrane.[50] Due to their mode of action, AMPs are less likely to induce resistance or tolerance in the cell, compared to traditional antibiotics.[51] Developing resistance to AMPs would require the bacterium to completely change or remodel their membrane structure.[42]

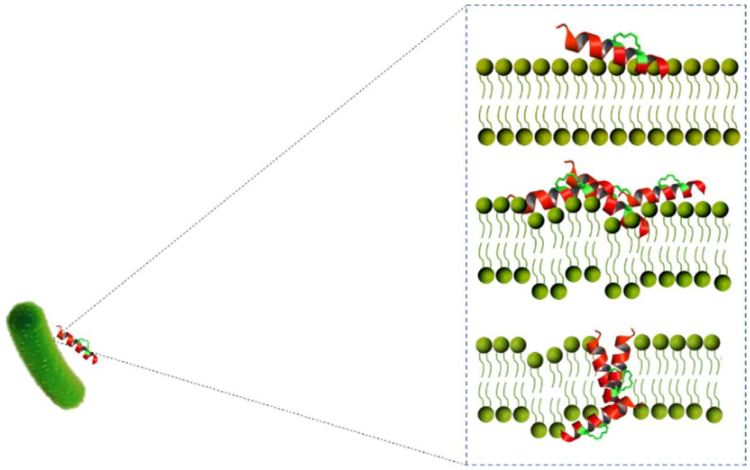

Figure 7. Simplified schematic of antimicrobial peptide mechanism of action through damaging the bacteria cell membrane and succeeding pore formation.

One important property of AMPs is their target specificity. Bacterial membranes are mainly comprised of anionic phospholipids that carry a net negative charge and are therefore susceptible to interaction with the positively charged AMPs.[49] The membranes of human cells, on the other hand, mainly consist of zwitterionic phospholipids and are enriched in cholesterol which results in a less negatively charged membrane and hence less affinity to AMPs.[52]

A cationic AMP, RRPRPRPRPWWWW-NH_2 was used in this thesis to modify substrates to create contact killing surfaces. The peptide consists of a hydrophilic sequence rich in proline and arginine amino acids followed by hydrophobic tryptophan residues. The RP side chain provides a positive net charge responsible for bonding to negatively charged membranes, while the hydrophobic modification by W, has shown to facilitate peptide penetration into the lipid membrane.[53]

4.2.3 Covalent immobilization of antimicrobial peptides

Although AMPs have shown unique and attractive properties for use as antibacterial therapeutic options, some complexities need to be addressed to bring peptide-based pharmaceuticals into clinical use. In release-based approaches, the effective control of the release concentration of incorporated peptides is challenging and most of the time after being released into physiological environments, they show decreased activity due to rapid protease digestion and peptide aggregation and their function is lost within a short time.[54,55] Sometimes a high concentration of peptides that is used to compensate for their short half-life, can cause cytotoxicity. Covalent immobilization of AMPs onto substrates is a suggested method that has shown to effectively enhance their long-term stability and decrease their toxicity towards host cells. Antimicrobial properties of AMPs covalently bonded to substrates can be preserved for a longer period and those surfaces have shown to have a broad spectrum of antibacterial activity.[56–60]

4.2.4 Elastin-like polypeptides

Elastin in its natural form, is a key extracellular matrix protein that is predominantly found in connective tissue and responsible for resilience and elasticity of tissues such as skin, ligaments and lungs etc.[61] Protein engineering approach has made it possible to design and produce elastin-like polypeptides (ELP) with similar properties as natural elastin, as well as to have a precise control over the properties of the final protein for use in medical applications.[62] Moreover, protein engineering, makes it possible to incorporate specific individual amino acids into the protein sequence for further chemical modifications.[63] ELP is synthesized by an initial translation of a desired sequence of amino acids encoded into a plasmid using living organisms such as bacteria. From *Escherichia coli* cultures, ELP can be expressed and purified in a large scale, Figure 8.

Cell-adhesive sequences (for example Arg-Gly-Asp, RGD) can be incorporated into ELP initial sequence to improve cell attachment properties for applications that demand proper tissue integration. It has been shown that ELP surface coatings functionalized with RGD sequences favor cell interaction and can promote osseointegration and bone formation.[64] ELP is thus considered as a promising material for biomedical applications.

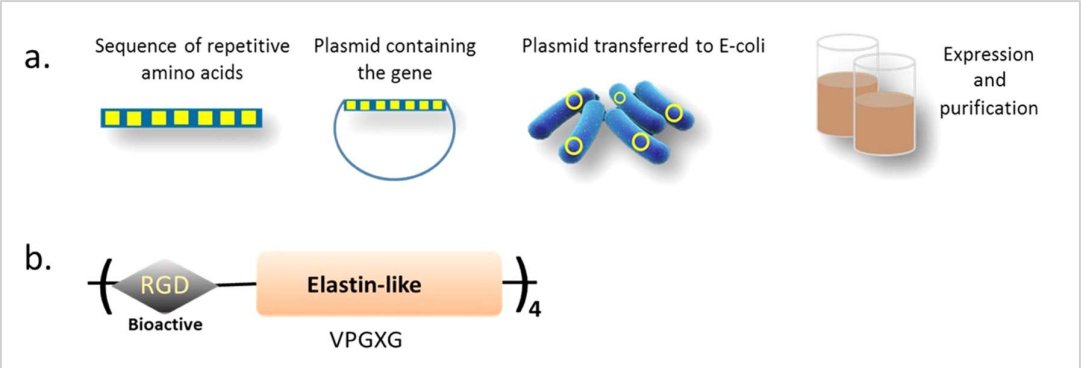

Figure 8. a, Schematic of steps in expression and purification of ELP from E-coli culture. **b,** Proposed ELP structure modified with bioactive RGD sequences.

The ELP thin films used for covalent immobilization of AMPs in this thesis, which is discussed in paper III, is a block copolymer synthesized recombinantly in *Escherichia coli* culture. Its structure contains four repeats of an elastin-like sequences and an extended fibronectin RGD sequence as cell-adhesive domain, as shown in Figure 8. A photo crosslinker is conjugated to the incorporated lysine amino acid residues, to provide a photo-crosslinkable ELP for fabrication of robust thin films followed by UV-exposure. It has been shown previously that ELP thin films can retain their bioactive functionalities after UV crosslinking.[63–65]

4.2.5 MF127 hydrogel

Lyotropic liquid crystals (LLC) can be cross-linked and used as soft ordered hydrogels. LLCs are formed when amphiphilic molecules, such as a block polymer with alternating hydrophilic-hydrophobic blocks, through interaction with surrounding solvent molecules self-assemble into ordered nanoscale aggregates.[66] Depending on factors such as concentration and chemistry of the amphiphile, temperature and the type of solvent, LLCs having different geometries ranging from example micellar phase (L_1), micellar cubic phase (V_1), hexagonal (H_1) and lamellar phase (L_a), see Figure 9, can be formed.[67,68]

Liquid crystalline hydrogels made from polymers exhibit unique properties originating from both network structure of the polymer and LLCs. Such hydrogels can swell and hold a large amount of water while maintaining their structures and can be considered in the development of platforms for variety of biomedical purposes.[69]

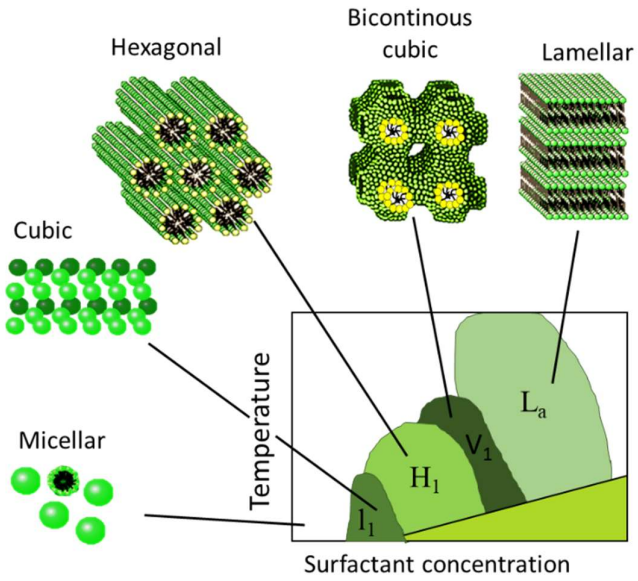

Figure 9. A schematic phase diagram for an amphiphile in water showing different micellar and LLC phases at specific amphiphile structure and temperature.

The hydrogels used in this thesis are covalently crosslinked LLCs made of pluronic™ diacrylated F127. The hydrogel has a micellar cubic phase, as shown in Figure 10, according to F127 phase diagram.[70,71] Covalent immobilization of AMPs to such structure, can form a soft three-dimensional antibacterial hydrogel with high liquid absorption properties. Moreover, these hydrogels have an amphiphilic character along their structure and can expose their hydrophilic sites for covalent attachment of AMPs. The hydrophobic parts of the hydrogels also provide hydrophobic interaction with amphiphilic AMPs, which is speculated to improve their immobilization and stability.

These hydrogels address the most important criteria of a proper wound dressing as they are capable of absorbing and preserving moisture to create a suitable environment in the wound and facilitate wound healing and increase comfort.[72–74] In addition, such hydrogels are non-toxic and biocompatible and do not expose any adverse effects on the wound and its surrounding.

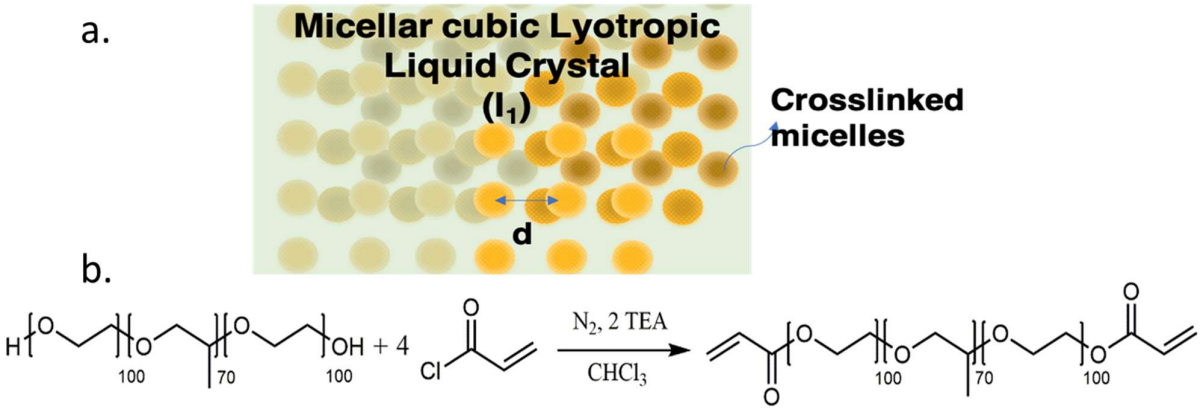

Figure 10. a, Schematic of a micellar cubic LLC phase, the structure of the hydrogel used in this work **b,** Chemical reaction showing the synthesis of the modified Pluronic F127. TEA stands for triethylamine.

5 *Experimental*

The experiments performed in this thesis are presented in three sections. The first part is focused on use of mesoporous titania thin films as antibiotic carriers for local drug release induced by diffusion (paper I), and controlled release using near infrared light (NIR) as an external stimulus (paper II). The second part of the experimental is focused on covalent immobilization of antimicrobial peptides (AMPs) onto substrates to create contact killing surfaces. The experiments were focused on attaching AMPs onto surface coating with RGD motives to create a bioactive contact-killing surface as implant coatings (paper III), and onto soft polymeric hydrogels to create bactericidal wound patches (paper IV). The third part introduces the analytical methods used for evaluation of the formed materials and their properties.

5.1 Formation of drug-eluting surface coatings

5.1.1 Mesoporous titania thin film preparation

Cubic mesoporous titania with pore sizes of 4, 6, and 7 nm were formed by the evaporation-induced self-assembly method (Figure 11). Pluronic® P123 (triblock copolymer $EO_{20}PO_{70}EO_{20}$) and cetyltrimethylammonium bromide (CTAB) ($CH_3(CH_2)_{15}N(CH_3)_3Br$), were used as structure directing agents. Larger pores (7 nm) were formed by using an organic additive, polypropylene glycol (PPG, M_n~4,000), which functioned as a swelling agent. A titania precursor solution was prepared by adding 2.1 g titanium (IV) ethoxide (20%) to 1.6 g concentrated hydrochloric acid (37%) under vigorous stirring, forming a homogenous solution. The amphiphile (0.5 g) was separately dissolved in 8.5 g ethanol under vigorous stirring followed by mixing with the precursor solution. The final solution was left to stir overnight to achieve a homogenous mixture. To obtain uniform thin films of mesoporous titania, 100 µL of the final solution was spin-coated (7,000 rpm) for 1 min on glass slides (2×2 cm), titanium discs (8 mm diameter and 3 mm thickness) and Ti-coated QCM-D sensors using a Spin150 spin-coater. The coated substrates underwent aging for 1 day at room temperature to obtain complete self-assembly. When the swelling agent was used, a moderately humid environment (RH=54%) was provided by a saturated KNO_3 aqueous solution in a refrigerator (T=4°C±1°C) during the aging process. Finally, the films were calcined by heating with a heating ramp of 1°C/min to 350°C, at which

temperature they were left for 4 hours to remove the template and to cross-link the titania. Nonporous titania thin films were formed as control samples using the same procedure, but without the addition of amphiphiles. To obtain hydrophobically modified MPT thin films, the substrates were treated in 5% dichlorodimethylsilane (DCDMS) for 1 hour.

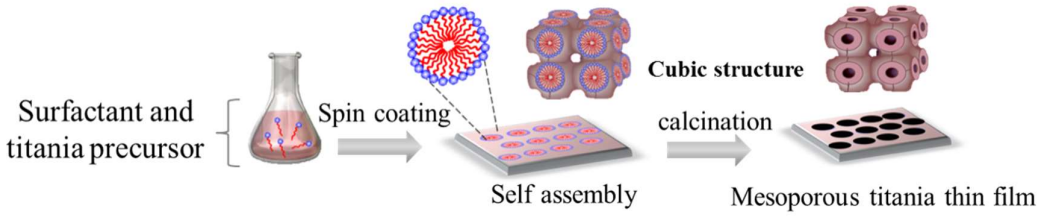

Figure 11. Schematic of the fabrication procedure to form cubic mesoporous titania thin films using the evaporation induced self-assembly method.

5.1.2 Antibiotic loading of MPT thin films

Substrate immersion was used to load MPT with antibiotics. The surfaces were immersed in antibiotic solutions for 1 hour. Vancomycin and gentamicin were dissolved in water (1 wt%) and Daptomycin was dissolved in methanol (1 wt%). DCDMS-treated (hydrophobic) mesoporous thin films were used to load Daptomycin, and the non-modified surfaces (hydrophilic) were used for Gentamicin and Vancomycin.

5.1.3 Polymer thin film synthesis with incorporated GNRs

To synthesize poly(N-isopropylacrylamide) (PNIPAAm) homopolymers, 1 g NIPAm was first purified by recrystallization in hexane prior to use. Then, the NIPAm was mixed with 0.0354 g of Azobisisobutyronitrile (AIBN) (mole ratio 1:41 to monomer) and 20 mg of 2-hydroxy-4-(methacryloyloxy) benzophenone (weight ratio 2% to monomer). The reactants were dissolved in 1 ml of ethanol, then kept under gentle stirring for 15 min. Later, the obtained solution was transferred to a flask with a septum and purged with nitrogen for 5–10 min to remove oxygen. The flask was then immersed in an oil bath at 60 °C and allowed to react for 60 min. The reaction was terminated by opening the flask to air, and the flask was stored in the fume hood

overnight at room temperature. The polymer was obtained in gel form and purified by continued washing with milli-Q water to remove unreacted excess reagent. Poly(N-isopropylacrylamide) copolymerized with acrylamide (PNIPAAm-AAm) was synthesized by adding 50 and 100 mg of acrylamide (5% and 10% weight ratio to NIPAM). The synthesis procedure was the same as mentioned above for the pure PNIPAAm.

Gold nanorods with a diameter of 10 nm and a length of 45 nm providing a SPR peak absorption of 850 nm were purchased from Nanopartz inc. CO, USA. The GNRs were modified with poly(ethylene glycol) (PEG) prior to the experiments to improve their biocompatibility and dispersibility.[75] In brief, the purchased solution of gold NRs contains the surfactant cetyltrimethylammonium bromide (CTAB). Excess CTAB was removed by centrifuging, decanting, and resuspending the particles in milli-Q water. Later, 200 µl of 5 mM PEG was added to a 1 ml of GNRs solution (2.8 nM), and the mixture was stirred for 24 h at room temperature. The resulting mixture was dialyzed the next day to remove any unreacted PEG.

5.1.4 Bacteria culture and growth

S. aureus (ATCC 25923) and *P. aeruginosa* (ATCC 35984) were used to study the bacterial attachment and growth on the mesoporous titania with different pore sizes both with and without incorporated antibiotics. One day prior to the experiment, a tube of 5 mL tryptic soy broth (30 g/L, Sigma) was inoculated by a single isolated colony from cultured agar plates of each bacterium. The inoculated cells were cultured in a shaking incubator at 200 rpm for 18 hours at 37°C until they reached stationary phase. The optical density of the bacterial suspension was adjusted to 0.52 at 620 nm (estimated to give 10^9 colonies) using a plate reader (Spectramax M3 Multimode Microplate Reader; Molecular Devices LLC, Sunnyvale, CA, USA).

Each bacterial solution was diluted at a ratio of 1:100 using simulated body fluid supplemented with 1% fetal bovine serum (FBS), and the mesoporous titania samples were seeded with 1 mL of the diluted solution. The samples with bacteria were then cultured for 1 hour in an incubator (ambient air) at 37°C to promote the attachment of the bacteria onto the titania surfaces. After 1 hour of culturing, media containing the unattached planktonic bacteria was aspirated. The samples were rinsed once with PBS and fresh media (simulated body fluid +1% FBS) was placed onto each sample. Samples were cultured for another 47 hours and at the end of this time period, they were rinsed three times with PBS. Each sample was placed inside a sterile 15 mL centrifuge tube filled with 2 mL of PBS. Samples were vortexed at 3,000 rpm for 2 min to release adherent bacteria into the PBS solution. Afterward, each bacterial solution was diluted twice, 1:10, and then each dilution was plated as five 10 µL spots onto sterile tryptic soy broth agar plates. Agar plates were placed inside an incubator at 37°C and 5% CO_2 for colonies to

grow. The colonies on each plate were counted and the total number of colonies per milliliter of vortexed solution was calculated and converted to colony- forming units/ml.

5.1.5 *In vitro* bacterial growth inhibition test

In paper II of this thesis, Staphylococcus epidermidis (ATCC 35984) was used to assess the bacterial growth around PNIPAAm-coated surfaces loaded with Vancomycin. 3 groups of substrates including: 1. substrates coated with MPT PNIPAAm loaded with Vancomycin, 2. substrates coated with MPT and PNIPAAm with incorporated GNRs and 3. substrates coated with MPT and PNIPAAm with incorporated GNRs and loaded with Vancomycin were placed in set of Petri dishes inoculated with Staphylococcus epidermidis. For groups 1 and 3, the substrates were loaded with Vancomycin by immersing the entire substrate in Vancomycin solution (0.2 mg/ml) for 24 h. The next day, the substrates were removed, then dried gently with nitrogen gas. Later, the substrates were saved in 12 well plates and kept in the fume hood for storage before the bacterial tests.

5.2 Covalent immobilization of AMPs onto ELP

5.2.1 Expression and purification of ELP

ELP containing RGD sequences was expressed recombinantly in Escherichia host, as described previously.[64] A plasmid encoding the elastin-like and RGD sequences was transformed into the E-Coli host and isopropyl β-D-1 thiogalactopyranocide (Sigma) as T7-lac promoter was added to induce the expression. After culturing, the bacteria were lysed, and the protein was purified using repetitive centrifuge cycles at above and below the lower critical solution temperature of the ELP (4°C and 37°C). The purified ELP was dialyzed, freeze dried and stored at 4°C.

5.2.2 ELP thin film preparation

A photo-reactive heterobifunctional N-hydroxysuccidimide ester-diazirine crosslinker (NHS-diazirine, succinimidyl 4,4'-azipentanoate, Pierce Biotechnology) was dissolved in DMSO (2 mg/mL) and mixed with a solution of ELP in PBS (2 mg/mL). The reaction was incubated for 2 hours and 1M tris buffer was added to the solution to stop the reaction. The diazirine conjugated ELP was dialyzed against DI water, frozen and lyophilized. All ELP coated surfaces mentioned subsequently, refers to this photo-crosslinkable form of ELP modified with diazirine. Microscope glass coverslips (VWR,15 mm) were cleaned using basic piranha solution. The polished titanium discs (grade 4, 8 mm in diameter and 3 mm in thickness) were rinsed with 70% ethanol followed by sonication. All substrates were dried with N_2 gas and stored at 4°C before ELP deposition. A 50 mg/mL (5 wt. %) solution of ELP in PBS was prepared at 4°C. The deposition of ELP onto the substrates was performed by spin-coating. For the glass substrates, 50 µl of the ELP solution and for the Ti discs 30 mL of the ELP solution was applied to the center of the surface and spun at 4000 rpm for 90 seconds. The spin coated substrates were treated by UV-light using a 365 nm, 8 W light source for 1 hour for ELP crosslinking. The crosslinked films were rinsed 3 times for 0.5 hour with PBS prior to the experiments to remove any non-crosslinked ELP.

5.2.3 Formation and modification of hydrogels (MF127)

A mixture of Pluronic F127 (30 wt%) and water (70%) was made to form a micellar cubic liquid crystalline phase according to the phase diagram[71]. Irgacure 2959 was added to the mixture of Pluronic F127 (2 wt%) as a photoinitiator. Mixing was performed in 20 ml glass vials manually using a spatula until a thick and homogenous gel formed. The gels were spread onto glass slides and kept in a sealed container overnight to set into ordered phase. The gels were then UV polymerized using a UV LED curing system (90 W, λ= 365 nm) for 10 min to form a flexible polymeric hydrogel with a thickness of 4-5 mm. The gels were cut into desired shapes and washed in milli-Q water for 48 h to remove the unwanted by-products and get into their fully swollen shape before further analysis and AMP attachment.

Pluronic F127 ($EO_{100}PO_{70}EO_{100}$) was chemically functionalized with polymerizable diacrylate head groups as previously reported.[70,76] The modified polymer was used for manufacturing of crosslinked F127 hydrogels for AMP modification. Briefly, acryloyl chloride was dissolved in chloroform (0.012 mol) and added dropwise to a mixture of Pluronic F127 ($EO_{100}PO_{70}EO_{100}$) (0.003 mol) and triethylamine (TEA) (0.006 mol) in $CHCl_3$ under N_2 atmosphere and magnetic stirring for 24h at RT. The mixture was then washed with the same volume of Na_2CO_3 solution (aq, 5wt %) for three times and dried over anhydrous $MgSO_4$ and the solvent was evaporated under reduced pressure to result in a white powder as final product (80% yield).

5.2.4 AMP immobilization onto ELP surfaces and hydrogels

A solution of antimicrobial peptide RRPRPRPRPWWWW-NH_2 (RRP9W4N, Red Glead Discovery AB, Lund, Sweden) was prepared in sterilized water to a concentration of 200 μM. For covalent attachment of AMP to the ELP surfaces, the ELP coated substrates were submerged into a solution of 1-ethyl-3-(3-dimethylaminopropyl) carbodiimide hydrochloride (EDC) and *N*-Hydroxysuccinimide (NHS) in MES buffer (pH=6) at a final concentration of 2 mg/mL and were allowed to react for 30 min slowly shaken at room temperature.

5.2.5 Bacteria culture

S. epidermidis (ATCC 35984)*, S. aureus* (CCUG 56489) and *P. aeruginosa* (CCUG 10778) were used to assess biofilm formation on the surfaces. A sterilized 10 μL loop was used to withdraw a single colony from cultured agar plates of each bacterium to inoculate a tube of 5 mL tryptic soy broth (TSB) one day prior to experiment. The inoculated cells were cultured in the incubator for 6 h, diluted in TSB and cultured in the incubator overnight to reach the stationary phase for bacterial growth.

The optical density of the bacteria culture was adjusted to 0.7 at 620 nm (estimated to give 10^9 colonies) using a spectrometer. The bacterial suspension was centrifuged for 10 min at 2500 rpm and the formed bacteria pellet was suspended in the fresh TSB media. 2 mL of the suspension was seeded onto the glass substrates, ELP coated substrates, activated ELP substrates and AMP functionalized ELP substrates in a 12 well plate. Bacteria were then cultured for 24 hours and 48 hours under standard culture condition (ambient air at 37°C) to promote biofilm formation onto the surfaces. For 48 hours' time point, after 24 hours of culture, the media was aspirated and replaced with fresh TSB for another 24 hours culture. At the end of each time point, surfaces were rinsed 3 times with fresh PBS to wash off any unattached planktonic bacteria before biofilm analysis. The same bacteria culture method has been used for materials involved in paper II, III and IV.

5.2.6 MRSA and MDR *E. Coli* culture

A single bacterial colony of MRSA (ATCC® 43300™) and MDR E. Coli (ATCC® BAA-2471™), isolated from cultured agar plates, were inoculated in a tube of 5 ml tryptic soy broth (TSB) and cultured in a shaking incubator at 37° overnight. The OD of the bacterial suspension was adjusted to 0.52 at 620 nm (estimated to give 10^9 colonies). To achieve a concentration of 10^6 CFU/ml the suspension was diluted 1000x further using TSB. Samples were placed in a standard 24 well plate and 1 ml of the bacterial suspension was used to seed each sample followed by incubation for 24 h under standard culture condition (5% CO_2, 95% air at 37 °C).

5.2.7 Evaluation of stability in serum

Fluorescent tagged AMP (5(6) carboxyfluorescein-RRPRPRPRPWWWW-NH_2) was used to study the stability of AMP attachment and its distribution on ELP surfaces after various duration of time. The tests were performed by incubating the fluorescent AMP functionalized surfaces in 20% human plasma serum (from 1 hour up to 3 weeks) and imaged using fluorescent microscopy.

Stability of AMP-hydrogels was tested upon incubation in human serum followed by bacterial assays using *S. aureus.* The tests were run in duplicate for 9 different time points. At each desired time point, the serum was removed, the gels were washed in PBS and bacterial assays were performed.

5.2.8 Zone inhibition

In order to show that the AMPs are covalently bonded onto hydrogels and they are not leaking into the bacterial culture, a zone inhibition test was performed. The bacteria culture was made in TSB at an optical density (OD) between 0.55 and 0.7. The bacteria pellet was collected by centrifuging at 2500 rpm and suspended in fresh 20 ml TSB (10^9 CFU). BHI agar plates were streaked with 100 μL of the bacterial suspension. The gels (2 of each hydrogel with and without AMP) was placed on top of the agar plates. As a second control, hydrogels submerged in same solution of AMP (200 μM) was prepared to show the leakage difference between covalent and physical attachment. The plates were incubated at 37°C overnight. Afterwards the zones around the gels where no bacteria were grown, were measured and compared between the samples. This inhibition zone area was considered as leakage of AMP from the hydrogels.

5.2.9 Bacterial live/dead analysis

Fluorescent microscopy with live/dead staining was performed to analyse the live and dead population of bacteria in contact with surfaces. The bacterial solution was removed from the hydrogels incubated in bacterial culture and the samples were gently rinsed twice with PBS. A drop of live/dead staining solution, LIVE/DEAD® BacLight™ Bacterial Viability Kit L7007, was placed on the top of the sample to cover its surface. The samples were incubated for 10 min at RT in a dark environment before the biofilm analysis.

5.2.10 Cell culture and growth

5.2.10.1 hMSC cell culture

Human bone marrow-derived mesenchymal stem cells (ATCC®_ PCS-500-012™) were sub-cultured according to supplier's instruction. Briefly, Dulbecco's Modified Eagle Medium (DMEM, Invitrogen, USA) containg GlutaMAX, 4.5 g/L glucose, 110 mg/ml sodium pyruvate, 10% fetal brovine serum and 1% penicillin/streptomycin was used to culture and expand cells at 37°C and 5% atmospheric CO_2. The following osteogenic supplements were also included in cell studies: 100 mM dexamethasone, 50 µg/ml ascorbic acid, and 10 mM β-glycerophosphate. Cells were pre-washed in DPBS before passaging by 0.05% trypsin-EDTA. Cells were seeded onto 12-mm Ti disks and placed in 24 well plates at a density of 10,000 cells/discs.

5.2.10.2 Mineralization assay

Calcium phosphate mineralization is an early-stage phenotypic marker of new bone formation. To run the mineralization assay, samples were seeded as previously described and rinsed in PBS (pH 7.4) and moved to new well plates. 1 ml of HCl (0.5 M) was added to each sample and left overnight on a rocker. Using Calcium o-Cresolphthalein Complexone (CPC) Liquicolor Test (Stanbio Laboratory, USA), the content of calcium was measured. Quantification of calcium content was done by correlating the calcium standard curve, obtained by absorption measurements at 550 nm, and dividing by substrate area to convert to calcium surface density.

5.2.10.3 Alkaline phosphate assay

Alkaline phosphatase (ALP) activity is one of the most widely employed markers for mid-stage osteogenic differentiation.[77] Since ALP is cellular ALP, its activity was quantified using the SIGMAFAST p-nitrophenyl phosphate tablet kit (p-NPP kit, Sigma Aldrich Co. St Louis, MO, USA), and normalized to total DNA content using the PicoGreen assay kit (Quant-iT PicoGreen, Molecular Probes). Samples were seeded with cells as previously described above, rinsed with PBS and moved to 24 well plates. A buffer containing 10 mM Tris (pH 8), 1 mM $MgCl_2$, 20 µM $ZnCl_2$ and 0.02 % Triton X-100 in deionized H_2O was added to the cell to lyse them. Samples were frozen at -80°C, thawed and assay was conducted. Double stranded DNA content was quantified by measuring sample fluorescence and according to instructions provided for the PicoGreen assay kit and compared to a known DNA standard curve. Same lysate was used to assay ALP activity. Lysate was mixed with a p-NPP solution (5 mM), while an ALP solution was mixed with serial dilutions of this p-NPP solution. Samples were incubated for 1h in room temperature in the absence of light. NaOH (3 M) was added to each well to stop the incubation and the absorbance at 405 nm was measured and correlated with the standard curve. The reported ALP activity has been normalized to total DNA content for each sample.

5.2.10.4 MTT assays

Primary fibroblasts (Gibco™ Human Dermal Fibroblasts, adult (HDFa)), were received from Fisher scientific, thawed and sub-cultured according to the supplier's recommendation. Briefly, cells were cultured and expanded in cell media with 1 Gibco™ Low Serum Growth Supplement Kit containing gentamycin/amphotericin solution with 10 % FBS at 37 °C and 5 % atmospheric CO_2. To perform MTT assays, hydrogel samples (thin hydrogel discs punched out with a 4 mm biopsy punch) were soaked in 1 ml DMEM for 3 days. 200 µl of the sample exposed media was added to the wells of a 96 well plate. As positive controls, media not exposed to any samples were used. The cell density of the fibroblasts was calculated with the help of a Bürker counting chamber. 5,000 cells were then added to each well. The well plate was incubated at 37 °C for 3 days. After 3 days of incubation, the media was aspirated from each well and replaced with 100 µl of fresh media (of corresponding type) to which 10 µl of the MTT solution (5 g MTT in 1 ml of PBS) was added and mixed gently by pipetting. The plate was put back into the incubator for 4h. 100 µl of the SDS solution (1 g of SDS in 10 ml of 0.01 M HCl) was added to each well and placed in the incubator for another 4 hours. The absorbance of each well was read at 570 nm by a spectrometer (Thermo scientific Multiskan GO). The negative control (media put through the MTT staining without any cells in it) absorbance was subtracted from each value and the viability of the cells were calculated by dividing of absorbance values by the mean of the positive controls. A value of 75% was considered as standard non-toxic sample.

5.2.11 Blood coagulation test (platelet count)

Prior to the experiment, blood collecting Eppendorf tubes, pipette tips and tubings to draw the blood, were heparinized to avoid unwanted blood activation. Heparinization was done by a layer-by-layer assembly method with alternating incubation with a polymeric amine and a heparin conjugate to obtain a double-coated heparin layer according to the Corline method (Corline Biomedical AB, Uppsala, Sweden).

Fresh blood from 2 healthy volunteers were collected in heparinized tubes containing 1 IU/ml of heparin solution (Leo Pharma A/S, Ballerup, Denmark). The blood was used fresh after sampling. 1 ml of blood was collected in an Eppendorf tube with 4 mM EDTA to be used as a reference point (named initial). Samples were conditioned by adding 1 ml of PBS and were shaken at 600 rpm for 30 min prior to the experiment. The hydrogels (control and AMP modified) were placed in heparinized 2.5 ml Eppendorf test tubes. 100 µL of PBS was added in order to soak the samples. Then 1 ml of fresh blood was added to each tube. The tubes were then rotated on an orbital shaker (incubating Waver, VWR) for 60 min at 37°C. As blank controls, 1 ml of blood was added to an Eppendorf tube without any hydrogels and treated with the same conditions. After the experiments, the blood was carefully collected from the tubes and mixed with EDTA giving a final concentration of 4 mM. The number of platelets were counted using a sysmex XP-300 hematology analyzer (Kobe Japan) directly after the experiment. Samples were run in duplicate with blood from each donor. Ethical approval was obtained from the regional ethics committee (Dnr:2008/264).

5.2.12 Pilot in vivo test

5.2.12.1 Animal handling

Seven female Sprague–Dawley rats (200–300 g) fed on a standard pellet diet and water were used in the study, which was approved by the Local Ethical Committee for Laboratory Animals (Dnr 1091/17). The animals were housed together (2–3 rats/cage) and were kept in an infection unit at the animal facility with daily supervision. Anasthesia was induced by isoflurane inhalation (4% with air flow of 650 ml/min) and maintained with continuous administration of isoflurane (~2% with an air flow of 450 mL/min) via a mask (Univentor 400 anaesthesia unit, Univentor, Zejtun, Malta). The back of the rats was shaved and cleaned with chlorhexidine (5 mg/mL; Fresenius Kabi, Norway). Six separate incisions were made on the back and pockets, into which hydrogel disks were inserted, were created by blunt dissection in the soft tissue under the skin.

5.2.12.2 Surgical Procedure

On the back of each rat, three control hydrogels and three AMP-hydrogels were inserted. The control hydrogels were inoculated by 50 µL of saline with and without *Staphylococcus aureus* (ATCC 25923) in two different dosage of 10^4 and $2x10^6$ CFU. The wounds were then carefully closed with intracutaneous sutures, followed by two to three simple sutures (Ethilon 5-0 FS-2, Eticon™, Johnson & Johnson, Scotland). The back was cleaned with saline and each rat received analgesics at a dose of 0.03 mg/kg (Temgesic®, Reckitt Benckiser, UK).

After 24 h and 72 h, the animals were sacrificed with an overdose of pentobarbital (60 g/L, APL, Sweden) after a short anesthetic induction with isoflurane. The back of the rats was cleaned with chlorhexidine and all the sutures were removed. The implants were retrieved, and the exudates were obtained from the pockets by repeated aspiration (5x) with 500 mL phosphate buffered saline (PBS) and kept on ice to study CFU and bacterial viability.

5.3 Analytical methods

5.3.1 Material and surface evaluation

5.3.1.1 SEM and TEM

In scanning electron microscopy (SEM), a beam of focused electrons is scanned over a solid sample to give highly resolved images. The highest resolved images are obtained by detecting the signal from the secondary electrons that originate from the surface. In transmission electron microscopy (TEM), an accelerated high energy beam of electrons passes through ultra-thin samples and creates a high-resolution image revealing the microstructural information. In paper I and II, SEM and TEM were extensively used for imaging the mesoporous titania thin films and powders. In paper II, SEM was used to evaluate the mesoporous titania and the polymer coating. In paper III, SEM was used to image ELP thin films and morphology of the bacteria in biofilms formed on surfaces. All samples in the second part were gold sputtered at a rate of 3 nm/min for 1 min prior to SEM imaging.

5.3.1.2. Small angle X-ray scattering

Long-range structural order within materials can be revealed by means of small-angle X-ray scattering (SAXS). The scattered X-ray patterns reveal information about long-range periodicity and mesoscopic dimensions of the samples. In paper I, mesoporous titania was grinded into a powder for SAXS measurements. The measurements were performed at MAX-lab, beam station I911 (Lund, Sweden) using synchrotron radiation (λ= 0.91 Å) and a two-dimensional Mar 165 CCD detector.

5.3.1.3. X-ray diffraction

X-ray diffraction is a method to determine the crystalline structure of a sample. When the sample is exposed to an X-ray beam, the atomic planes in the crystallites diffract the beam at certain angles with constructive interference of X-ray to fulfil the Bragg condition (Equation 1)

(Eq. 1) $$n\lambda = 2d\sin\theta$$

Where d is the lattice spacing, θ is the angle, n is an integer value and λ is the wavelength of the incident beam. In paper I, the crystallinity of the mesoporous titania powders were evaluated by XRD. The X-ray diffractometer used was a Bruker D8 advance (Bruker Corporation, Billerica, MA, USA) with a radiation wavelength of 1.5405 Å (Cu $K\alpha$1 radiation).

5.3.1.4 Differential scanning calorimetry (DSC)

Determining the phase transition temperature (Tph) to identify the volume-phase transition behavior of PNIPAAm and PNIPAAm-AAm polymers was done in paper II. The Tph was defined by the point between the moment of increase in the DSC endotherm and the maximum of the DSC peak. For this purpose, a scanning calorimeter was used (Perkin – Elmer Instruments, USA). In this test, 5 mg of polymer was immersed in milli-Q water for 1 day to reach the equilibrium state. Later, the samples were sealed in aluminum pans and scanned from 22°C to 45°C under a dry nitrogen atmosphere at a heating rate of 1°C/min.

5.3.1.5 X-ray photoelectron spectroscopy

X-ray photoelectron spectroscopy (XPS) also known as electron spectroscopy for chemical analysis (ESCA) is a surface sensitive analysis technique to determine the chemical composition of a surface. Low energy X-rays irradiate the sample and the binding energy and intensity of the photoelectrons leaving the sample allow for identification and quantitative determination of the elements present at the surface of the sample. In part 1 of the thesis, XPS was used to examine the surface composition of mesoporous titania thin films before and after modification and drug loading. In part 2, XPS was used to evaluate the ELP thin films before and after surface activation with EDC and NHS. The equipment used was a Quantum 2000 scanning microscope (Physical Electronics, Inc., Chanhassen, MN, USA) with a 100 μm point diameter at a 5 nm analysis depth.

5.3.1.6. Atomic force microscopy

Atomic force microscopy (AFM) is a scanning probe microscopy method to measure local properties of a surface such as its roughness through interactive forces. In paper I, AFM was used to measure the surface topography of the mesoporous titania films. The measurements were performed in semi-contact or intermittent mode at two different scan sizes (1 and 0.5 μm). A conical tip with a length of 200 nm and a radius of 5 nm attached to an NT-RTESPA cantilever was used to scan the samples. The AFM used was an NT-MDT model (Moscow, Russia).

5.3.2 Antibiotic release, AMP attachment and stability evaluations

5.3.2.1 QCM-D

Quartz crystal microbalance with dissipation monitoring (QCM-D) is a mass sensitive analytical technique. Upon application of an AC voltage, a thin quartz crystal attached to a pair of gold electrodes, starts to oscillate at its acoustic resonance frequency. The mass uptake or release at the sensor surface causes changes in the resonance frequency (Δf) as a function of time. Δf can be converted to rigid mass adsorbed or desorbed (Δm) by applying the Sauerbrey equation (Eq. 2).

$$\Delta m = -\frac{\Delta f \times C}{n} \qquad (Eq.\,2)$$

, where C = 17.7 ng Hz^{-1} cm^{-2} for a 5 MHz crystal and *n* is the overtone resonance number. Moreover, an energy dependent property of the surface, the dissipation (D) can be measured by QCM-D. ΔD is correlated to the changes in viscoelastic properties of the adsorbed layer.

In paper I and II, QCM-D was used to measure the absorbed mass of the drugs within the mesoporous titania thin films. In addition, the accessible pore volume was calculated from the amount of deuterium oxide (D_2O) that was absorbed. In part 3, the adsorption and release behavior of antimicrobial peptides onto ELP surfaces before and after EDC/NHS activation were monitored by QCM-D and compared to pure Ti surfaces. The swelling ability of the ELP thin films was also measured by D_2O absorption tests. The instrument used was a Q-sense E4 and all samples were evaluated using titanium QCM-D discs (QSX 310, Q-sense).

5.3.2.2 Ultraviolet-Visible (UV-VIS) spectroscopy

Ultra-violet and visible radiation interact with matter which causes electronic transitions. This method is routinely used in analytical chemistry for quantitative determination of ions, compounds and macromolecules in solution. In paper II, phenol was selected as the drug model to evaluate the drug release from PNIPAAm-coatings in response to NIR irradiation by the use of UV/VIS spectroscopy (Agilent 8453, USA). PNIPAAm-coated glass slides (with or without GNRs). The coated and drug-loaded surfaces were placed in the bottom of UV-VIS cuvettes followed by adding 2 ml of milli-Q water. One cuvette was filled only with milli-Q water and used as a blank. The phenol absorbance was measured at a wavelength of 269 nm. Then, the samples were subjected to NIR light for 30 min. The absorbance was registered for each sample (n=4) at each data point. The standard calibration curve of the absorbance as a function of the phenol concentration was obtained at 269 nm (Appendix A). Results are presented as the mean value.

5.3.3 Bacterial attachment and viability evaluation

5.3.3.1 Fluorescence light microscopy

Fluorescence light microcopy (FLM), is used to image samples that are either fluorescently labeled or fluorescing in their natural form (autofluorescence). When fluorescent samples are irradiated with absorbable light of a specific wavelength, they can emit energy detectable as visible light. In this technique, the microscope filters out only the desired wavelength that matches the fluorescing sample. As a result, the electrons in the fluorescing specimen are excited to a higher energy level and when they relax, emit visible light. The emitted light reaches a second barrier filter to eliminate the residual background light from the specimen to pass to the eye or camera. Thus, the fluorescing sample shine out against a dark background

with high contrast. FLM was extensively used in this thesis to study the live and dead fractions of biofilms formed on substrates. The microscope used was a Carl Zeiss GmbH (Jena-Germany) equipped with an HBO 100 microscope illuminating system. Green filter, GFP, 38HE ($\lambda_{Excitation}$ = 470 nm and $\lambda_{Emission}$ = 525 nm) and red filter ($\lambda_{Excitation}$ = 545 nm and $\lambda_{Emission}$ = 605 nm) were used for imaging. The biofilms were stained using LIVE/DEAD® *Bac*Light™ Bacterial Viability kit (Molecular Probes, Invitrogen). The images were obtained with SYTO® 9 and propidium iodide nucleic acid staining provided in the kit. Live bacteria with intact cell membranes appeared green and dead bacteria with compromised membranes appeared red. The statistical data from live/dead bacteria obtained from red and green fractions of fluorescent microscopy images were presented by the mean value with standard deviation (paper I and II).

All the experiments were performed three times with two replicates. 20 images from each surface were used to obtain the image analysis data. FML was also used to image fluorescent tagged antimicrobial peptides to study their stability in serum condition (paper III).

6 *Results and discussion*

The results that are presented and discussed in this thesis are divided into two parts. The focus of the first part is on the evaluation of the antibacterial performance of mesoporous titania thin films and their function as antibiotic delivery systems in two drug release approaches: a diffusion-based drug release from mesoporous titania thin films with variable pore sizes and hydrophobicity (paper I), and a photon-induced controlled release system from mesoporous titania films embedded in polymer PNIPAAm with incorporated gold nanorods (paper II).

In the second part, the antibacterial performance and evaluation of contact-killing surfaces are in focus. Such materials are designed by covalent immobilization of cationic AMPs onto suitable substrates including elastin-like polypeptides with cell-adhesive RGD motives to create bioactive antibacterial implant coatings (paper I) or onto an ordered soft polymeric hydrogel to be utilized as absorptive antibacterial wound patches (paper II).

6.1 Antibacterial properties and drug-release from mesoporous titania thin films

6.1.1 Evaluation of mesoporous titania thin films

The morphology of formed mesoporous titania thin film (MPT) on titanium substrates was visualized by SEM. SEM micrographs presented in Figure 12 show an evenly distributed porous structure with pore accessible from the surface. Moreover, SEM was used to image MPTs in combination with thin polymer layer on top with incorporated gold nanorods (GNRs). The SEM images showed a well-defined porous structure with a pore size of 6 nm covering the whole titanium surface protected by a 200 nm polymer film with incorporated GNRs (Figure 13a). A homogenous distribution of GNRs was observed which is crucial to preserve the absorption of NIR light in the polymer film. The film thickness was measured by cross-section analysis, which was ~200 nm for the ones formed using pluronic P123 and CTAB and ~700 nm when the swelling agent PPG was added to P123, Figure 12b. The increase in the film thickness can be explained by the increased viscosity of the coating solution by adding PPG, resulting in a thicker film upon spin coating. The thickness of the MPT- PNIPAAm was a total of 500 nm, which consisted of 300 nm MPT and 200 nm PNIPAAm layer (Figure 13).

The average pore sizes of MPTs formed with different templates were calculated using image analysis of SEM and TEM micrographs and are shown in Table 1. The pore volumes of the films were calculated by the QCM-D data obtained from H_2O/D_2O exchange experiments using the mass difference between water and heavy water. As expected, the volume increased with increasing pore size and increased film thickness and the size/volume of the formed pores correlates well with the size/volume of the templates used in the synthesis. The overall results from evaluation of MPT suggest a versatile structure with tunable pore sizes and pore volumes that enable loading of drugs having different size.

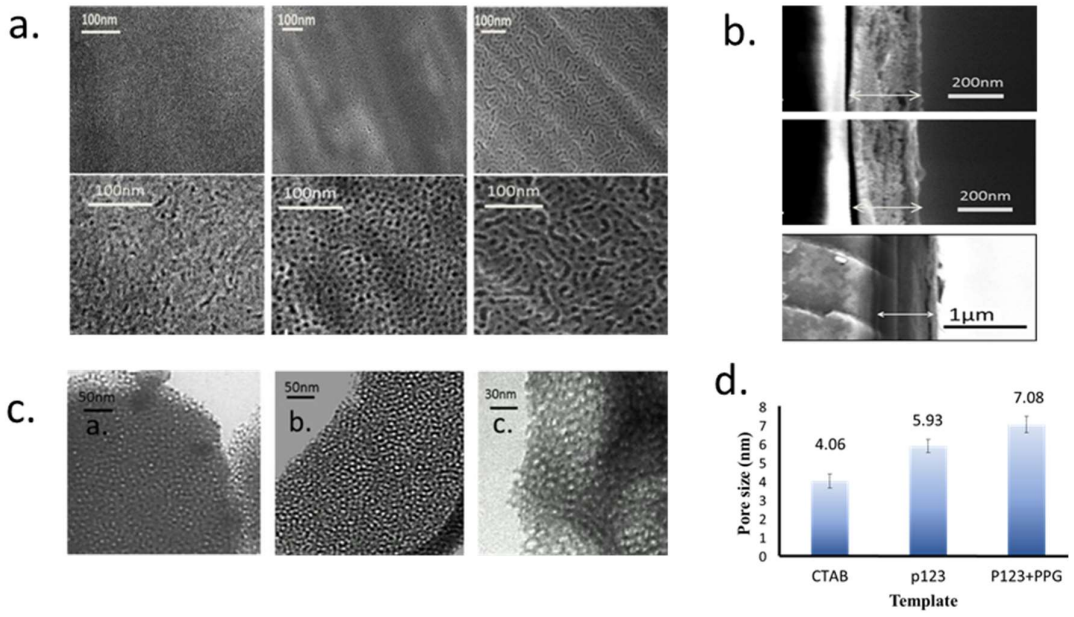

Figure 12. **a,** SEM Micrographs of mesoporous titania thin films formed using different templates; from left to right CTAB, P123 and P123+PPG (1:1). **b,** SEM images of the cross-section of mesoporous titania coatings, CTAB, P123 and P123+PPG (1:1) from top to bottom. **c,** TEM images of mesoporous titania thin films scraped off from the substrates CTAB, P123 and P123+PPG (1:1) from left to right. **d**, A graph showing the pore sizes obtained from the TEM micrographs.

Table 1. Properties of mesoporous titania thin films including average pore diameter obtained from SEM images, the percentage of pore coverage on the surface calculated from SEM images and the pore volume of the mesoporous titania thin films accessible for water obtained from QCM-D measurements.

Template	**Average pore diameter (nm)**	**Pore surface coverage (±5%)**	**Pore volume (%)**
CTAB	4	18	75
P123	6	25	57
P123 + PPG (1:1)	7	42	55

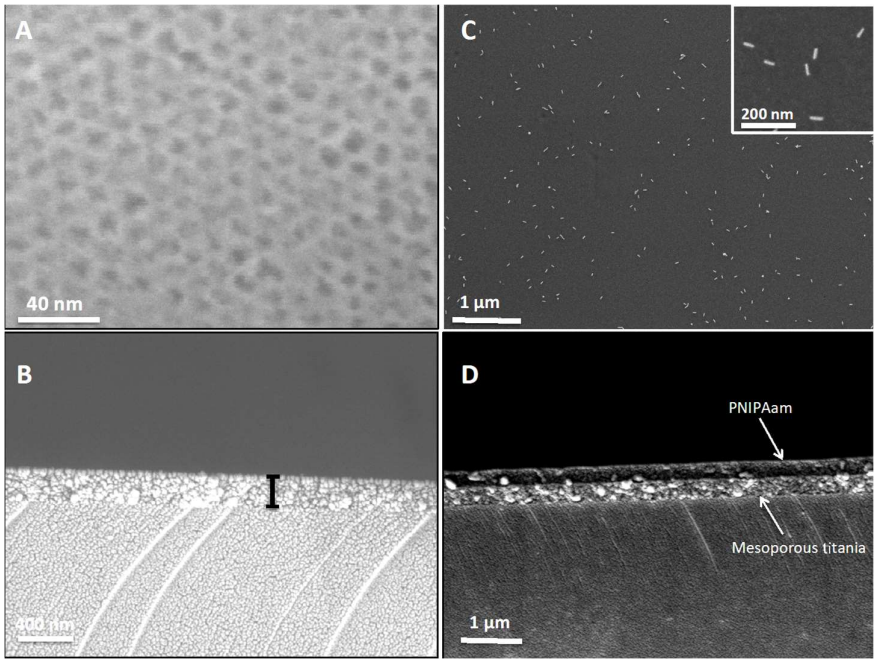

Figure 13. SEM image showing: **a,** Top view of the mesoporous titania (MPT) film. **b,** A cross section of mesoporous titania film, where the black line indicates the film thickness. **c,** Top view of the GNRs on the PNIPAam. The inset shows the rods at higher magnification and **d,** A cross section view of the MPT film and PNIPAAm layer.

When analyzed with SAXS, clear Bragg peaks with different intensities and at different positions were apparent in diffractograms for the mesoporous samples, while no peaks for nonporous sample were observed, Figure 14b. Relatively broad peaks indicate that the degree of order was relatively low, which is probably a result of the spin-coating technique used. It has been discussed before that thin films formed by dip coating instead of spin coating usually show higher degree of order while the films formed by spin coating are more homogenous in thickness.[78]

XRD results showed the formation of crystalline anatase TiO_2. The crystalline structure did not change by changing the pore sizes and was the same for all the samples including the nonporous. In Figure 14a, a representative diffractogram for the titania films is shown.

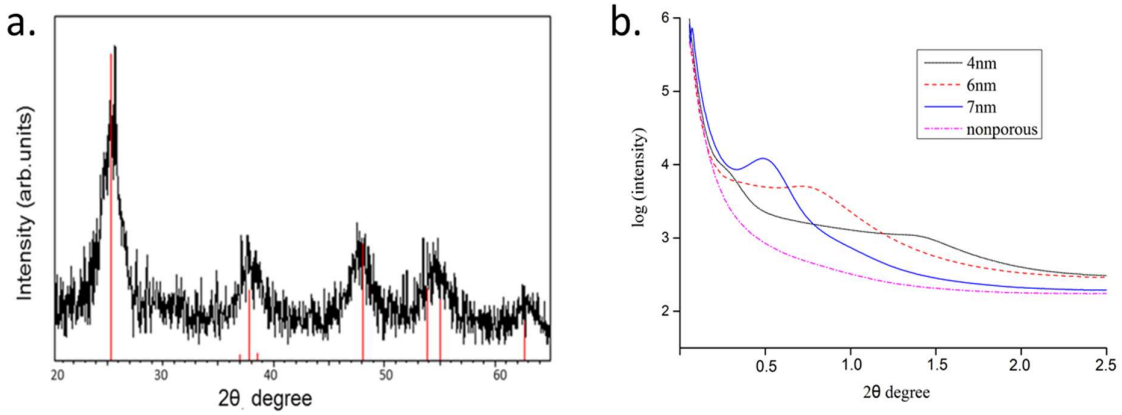

Figure 14. **a,** A representative XRD pattern obtained from mesoporous titania powders. **b,** SAXS diffractograms of mesoporous titania powders, see the graph legend for the sample names.

From the combined material characterization results it was clearly seen that the physical and chemical properties of the mesoporous titania thin films remained the same independently of pore size, a prerequisite for investigating the effect of pore size alone on drug loading and antibacterial responses.

6.1.2 Titania thin films and antibiotic delivery

When MPT thin films were loaded with antibiotics and the release was driven by diffusion upon rinsing with solvents, a high loading efficiency and fast release rates were observed according to QCM-D measurements, as is shown in Figure 15. The amount of drug loading correlated well with the pore size and accessible volume of the pores as measured by H_2O/D_2O absorption.

Since the release of the drugs from MPT thin films are mainly driven by diffusion from the pores upon rinsing with solvent, the burst release could not be controlled. The rinsing rate during the QCM-D measurement was set to 50 mL/min. This rate is considered to give rise to a much higher release compared to physiological conditions. Therefore, the results from the release kinetics cannot be directly transferred to the clinical situation. However, as discussed above a high initial release from antimicrobial coatings can also be useful to clear the environment around the implant from bacteria and prevent bacterial colonization in adjacent tissue.[4]

The dissipation did not change noticeably during loading of the drugs, indicating that no viscoelastic film was formed onto the mesoporous titania and that the adsorption of drugs is limited only to the pores.

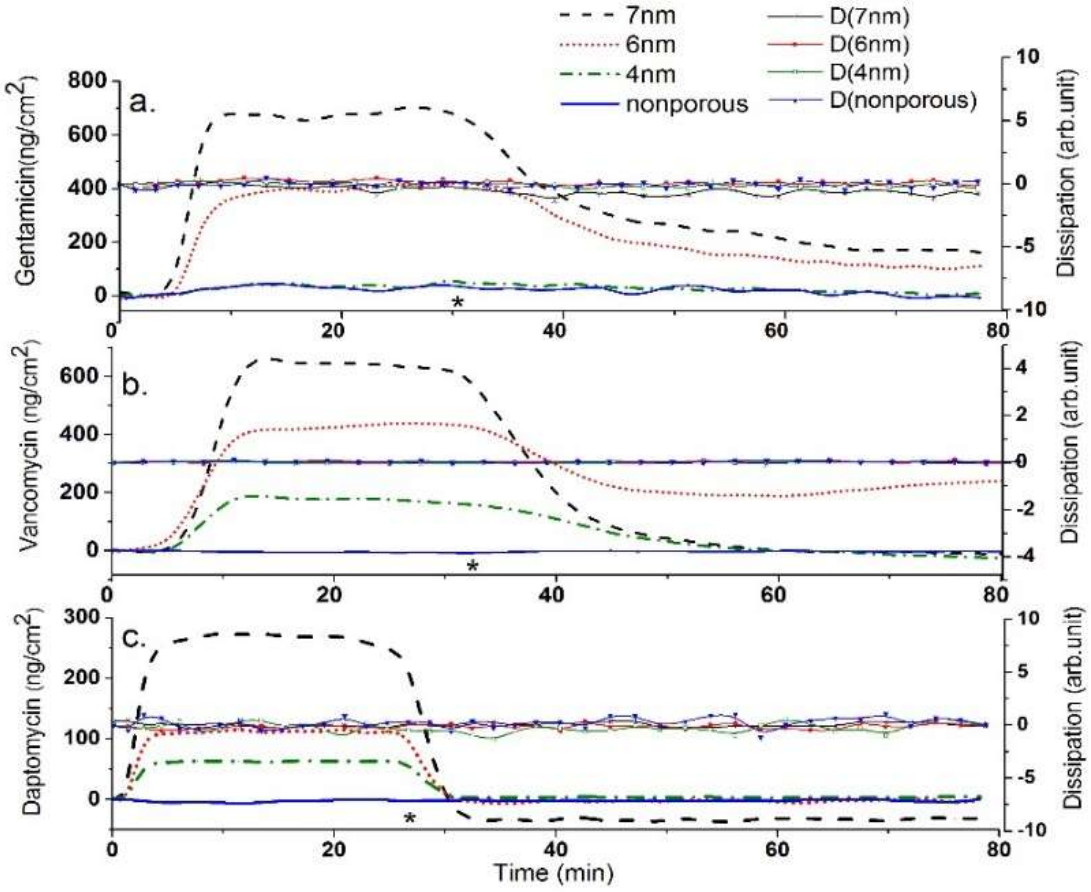

Figure 15. QCM-D recordings obtained from loading and release of the three different antibiotics: **a,** Gentamicin, **b,** Vancomycin, and **c,** Daptomycin from mesoporous titania with variable pore sizes (For Daptomycin DCDMS modified surfaces were used).
* Indicates start of rinsing with solvent to follow the release.

To control the burst effect and to be able to design a system that enables a controlled drug release, mesoporous titania thin films with pore size of 6 nm were coated with a layer of thermoresponsive PNIPM polymer with incorporated gold nanorods. Such system utilizes gold nanorods to generate heat upon absorption of light in the near infrared (NIR) spectrum. This amount of heat induces shrinkage of the PNIPAAm and thus release of the drug molecules. The use of NIR light as an indirect stimulus for drug release is claimed to be harmless to the body tissue, since light with such wavelengths can penetrate deeply without being absorbed by cells and hemoglobin.[79]

The results from differential scanning calorimetry (DSC) analysis showed that PNIPAAm containing 10% acrylamide had a phase inversion temperature of 42°C, Figure 16. This temperature is considered suitable for intended *in vivo* application and can be achieved by the heat generated from GNRs upon NIR radiation.

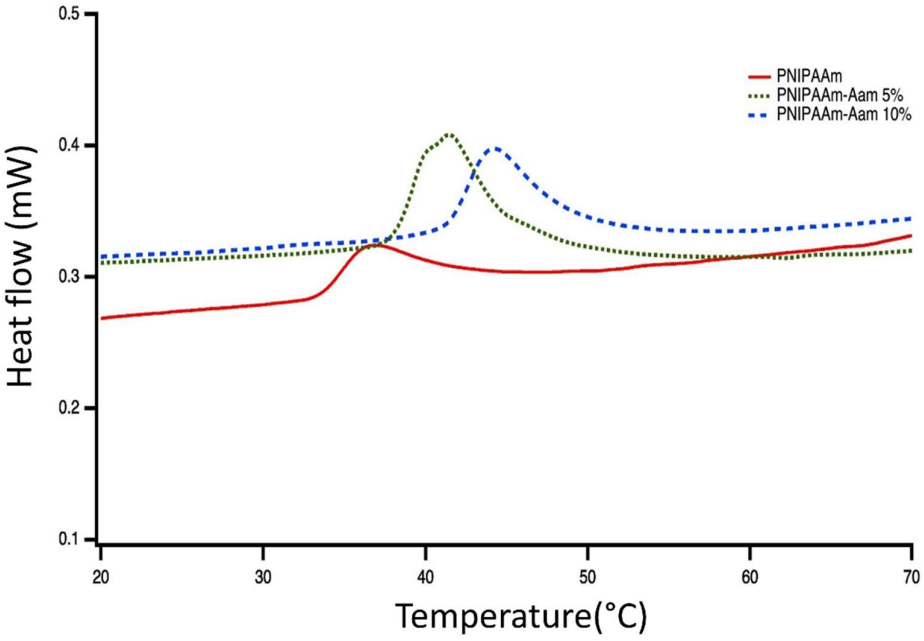

Figure 16. DSC scans of PNIPAAm and PNIPAAm-AAm polymers (at a heating rate of 1°C /min). All data is presented as a mean value (n=3).

Phenol was selected as a model drug to evaluate the drug-release of MPT- PNIPAAm-coated surfaces upon irritation with NIR by UV/VIS spectroscopy. No pre-leakage of phenol before irradiation was observed. Upon irradiation, the MPT- PNIPAAm surfaces that contained gold nanorods showed an immediate release of phenol. Such behavior is probably due to a sudden physical contraction of the thermoresponsive polymer as response to the heat generated by GNRs upon irradiation. Intriguingly, even after termination of irradiation, the release of phenol was continued, Figure 17. This indicates that the drug release from such system cannot be totally halted, but only initiated using NIR. However, the data from QCM-D measurements indicated that the polymer films can re-swell to their initial state before NIR irradiation. Thus, the continued release indicates some permanent change in the structure of the polymer induced by NIR. Thus, we could not claim a cycle of phenol release and uptake induced by NIR. In addition, the polymers with no GNRs, revealed a slight release of phenol upon irradiation both in UV/VIS and QCM-D measurements, suggesting some absorption of NIR by the polymer itself.

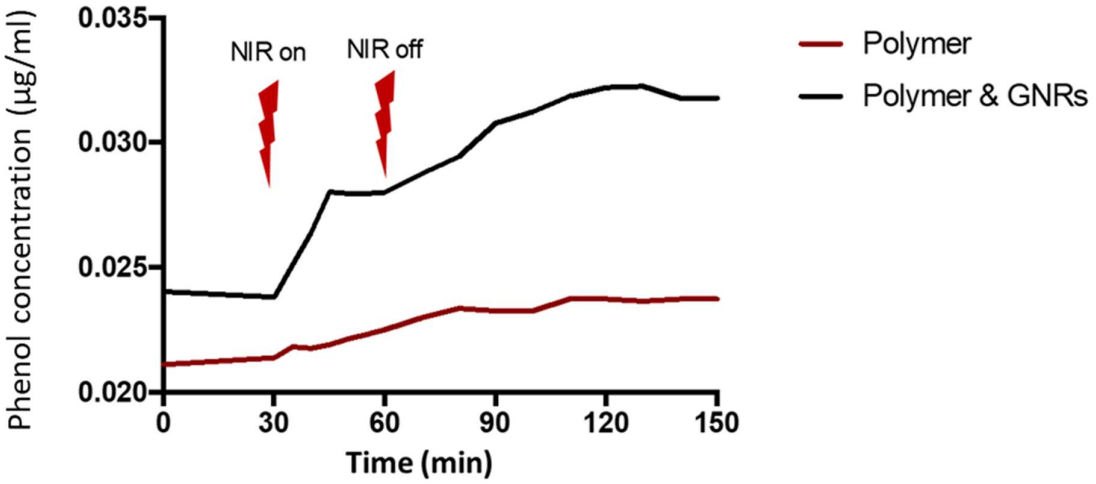

Figure 17. Changes in the phenol concentration upon irradiating the coated surfaces with NIR.

6.1.3 Bacterial assays for drug-delivery evaluation

The results from bacterial assays showed that mesoporous titania thin films can to some extent hinder bacterial growth without the presence of any antibiotic. The bacterial assays showed that the presence of pores alone can affect the growth of bacteria *S. aureus* and *P. aeruginosa* onto surfaces, Figure 18a. Further assessments are required to conclude if the decrease in bacterial adhesion is merely due to the change in surface energy and nanotopography of the substrates or the fact that changing these parameters can affect the absorption of serum proteins present in the media and therefore the subsequent bacterial adhesion. The lowest number of bacteria was found on hydrophobically modified MPT with a pore size of 4 nm. The results indicate that the bacterial attachment was generally lower when the surface energy was decreased.

When the MPT surfaces were loaded with different antibiotics, a more predictable pattern of decreasing bacterial attachment with increasing pore size was observed. According to our QCM-D results shown in Figure 15, more antibiotics was loaded into and released from MPT with bigger pore sizes. These results confirm that MPT films can potentially be used as tunable drug release coatings on implants to decrease the initial attachment of bacteria and subsequent biofilm formation. However, such release behavior is not controlled and sustained over a longer time period.

To further investigate the effect of the photoinitiated MPT-PNIPAAm system, Staphylococcus epidermidis (ATCC 35984) was used to assess the bacterial growth around the PNIPAAm-coated surfaces when loaded with the antibiotic Vancomycin. The results from a zone inhibition study, shows a clear inhibition zone around the radiated MPT-PNIPAAm with incorporated GNRs, while such zone was absent for all the other test groups upon irradiation (Figure 19). The inhibition zone indicates the release of Vancomycin from the MPT-PNIPAAm system and extended a couple of millimeters all around the sample. Since no inhibition zone was detected before irradiation, it can be concluded that polymer layer preserved the drug loading inside MPT and irradiation with NIR succeeded in initiating the drug release.

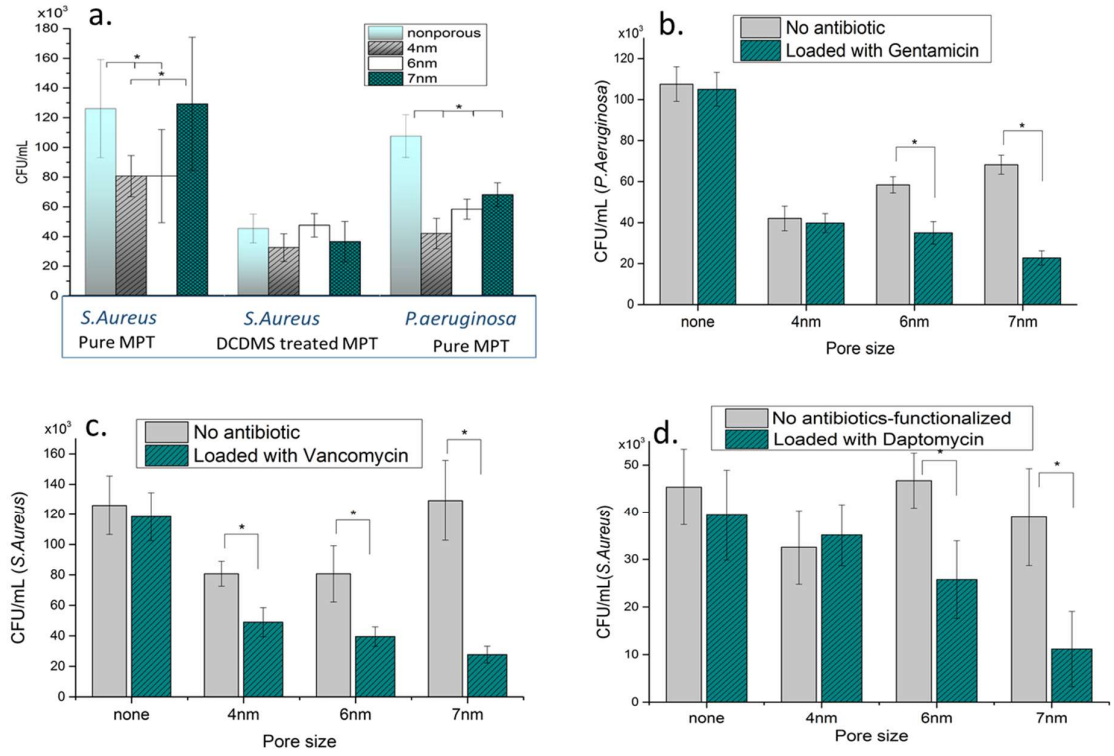

Figure 18. Data from counting the colony forming units grown on modified and unmodified mesoporous titania **a,** without the presence of antibiotics. **b,** with and without Gentamicin **c,** with and without Vancomycin **d,** with and without Daptomycin. Values are mean ±SD, N=3, *p<0.05 compared to mesoporous titania surfaces for each bacteria strain. MPT = mesoporous titania.

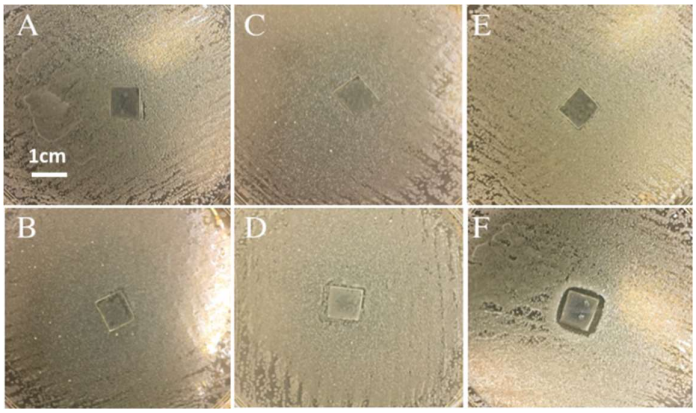

Figure 19. Representative images show zone of inhibition results for Staphylococcus epidermidis around the samples due to irradiation with NIR. PNIPAAm samples loaded with antibiotic, **a,** before and **b,** after irradiation, PNIPAAm samples incorporated with GNRs, **c,** before and **d,** after irradiation, and PNIPAAm samples incorporated with GNRs and loaded with antibiotic, **e**, before and **f,** after irradiation.

6.2 Antibacterial performance and evaluation of contact-killing surfaces

6.2.1 Material evaluation and AMP attachment

An alternative to drug-eluting surface coatings to combat bacterial colonization and subsequent infection on biomedical devices is to design contact killing surfaces. Such surfaces do not release any antibacterial drugs but rapidly kill bacteria upon contact. The contact killing surfaces in this thesis are based on covalent immobilization of AMPs onto different substrates using NHS-EDC coupling chemistry. Immobilization of antimicrobial peptides onto surfaces is suggested to be an effective approach to minimize their cytotoxicity and increase their long-term stability, which is needed for clinical applications.[80–83] In this thesis, EDC was used to activate carboxyl groups on the substrates to react with primary amine groups present in the AMP structure. The use of NHS improves the bonding efficiency and increases the dry-state stability after immobilization.[84] Two substrates for covalent immobilization of AMPs were chosen; photo-crosslinked ELP thin films with cell adhesive RGD sequences, and ordered nanostructured hydrogels made of cross-linked pluronic™ F127 block copolymers. The former substrates have previously been shown to favour cell interactions, enhance osseointegration and bone formation *in vivo*. Moreover, such thin films have enough mechanical strength to endure clinically relevant shear forces.[64] When such properties are combined with the antibacterial effect introduced by AMPs, it makes it an ideal candidate for use as bioactive antibacterial implant coatings. The F127 hydrogels on the other hand, possesses characteristics such as softness and high liquid absorption capacity and can maintain moisture in their structure. Such property is an important prerequisite of a wound dressing for a proper wound healing and soothing effect.[85,86] Hydrogels with such properties were therefore used in this thesis for AMP immobilization to develop contact killing surfaces suitable for wound-care application. The amphiphilic structures of hydrogels are speculated to be an ideal property to improve the stability of immobilized AMPs, since hydrophobic interaction between hydrophobic sites in hydrogel structure and hydrophobic domains of AMP molecules can help to form a stronger attachment. This speculation is based on Lukas Boge's work where it was demonstrated that AMPs can be immobilized within LLCs (in this case cubosomes) even without covalent attachment.[87]

SEM images of dried ELP coatings demonstrate a uniform coating on the microscale with porous structure in the nanoscale formed on Ti surfaces as shown in Figure 20b.

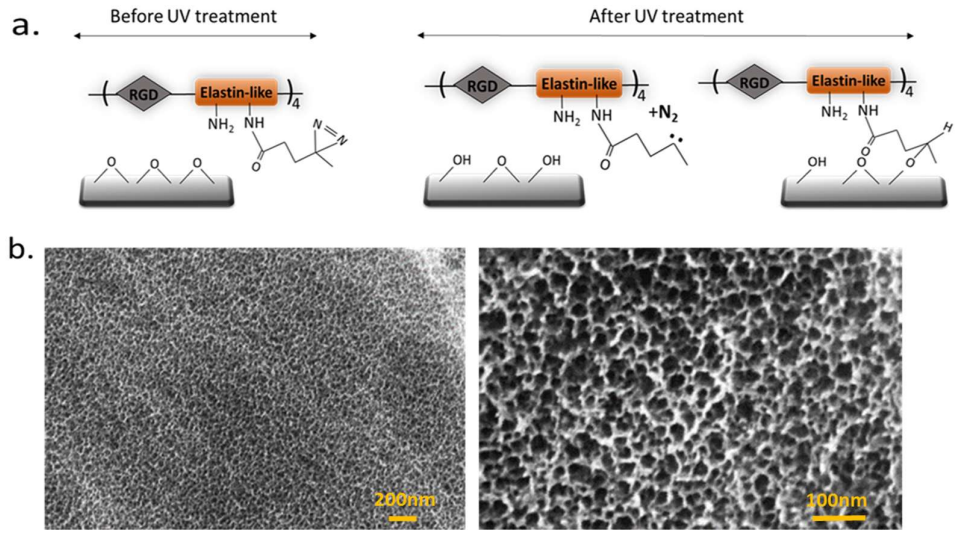

Figure 20. a, Proposed schematic model for conjugation of ELP onto Ti substrates using diarizine moiety. **b,** SEM of photocrosslinked ELP onto Ti substrate, the magnification increases from left to right.

The amphiphilic domains of the hydrogel are arranged in an ordered structure consisting of alternating hydrophilic and hydrophobic domains.[88] The SAXS data obtained from the hydrogel structures have shown highly ordered mesoscale structure of hydrogels indicating that lyotropic liquid crystals have preserved their order after cross-linking throughout the gel.[70,76] Figure 21 is a photo taken from a 3D printed hydrogel mesh before and after water absorption (swelling).

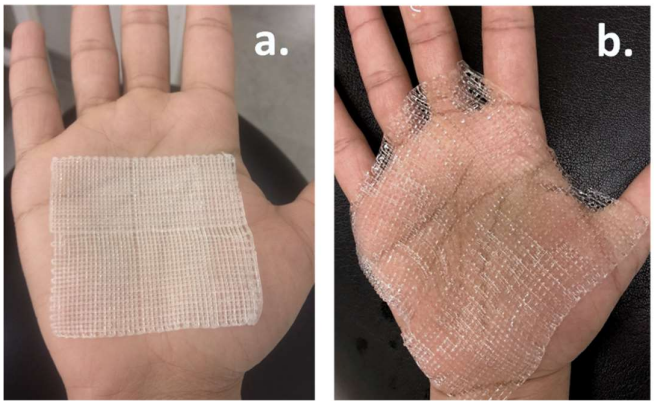

Figure 21. 3D printed hydrogel mesh a) before and b) after water absorption.

The EDC-NHS coupling is shown in Figure 22. According to XPS results shown in Table 2, EDC-NHS immobilization of the AMP, RRPRPRPRPWWWW-NH_2 did not introduce any impurities to ELP coatings before and after attachment.

RRPRPRPRPWWWW-NH_2, is a cationic peptide rich in proline and arginine amino acids that provide positive charge, and a hydrophobic tryptophan (W) rich tail. The positive net charge facilitates bonding to the negatively charged phospholipid head groups of bacteria membranes while the hydrophobic W tail is believed to limit the toxicity of the AMP to eukaryotic cells and allow deeper penetration into the interfacial region of negatively charged membranes.[53,89–91]

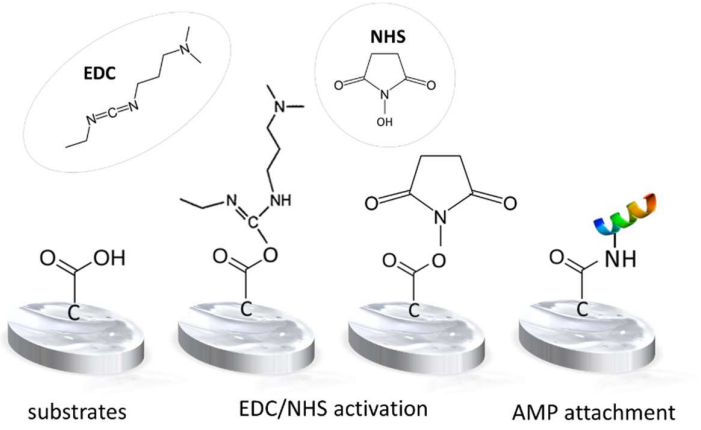

Figure 22. A demonstration of AMP binding onto substrates (ELP coatings/ F127 hydrogels) by EDC/NHS activation.

Table 2. The atomic percentage (%) of the chemical composition of ELP thin films coated on Ti discs before and after AMP conjugation by EDC/NHS coupling, as measured by XPS.

	C1s	N1s	O1s	Ti2P
Titanium disk	0.75	0.29	55.80	43.16
ELP coated Ti	64.20	15.71	20.09	-
ELP Coated Ti + AMP	51.98	16.88	31.14	

QCM-D measurements were performed to investigate the stability of covalently bonded antimicrobial peptide into ELP substrates in comparison to when they are only physically adsorbed onto the ELP thin films. Considerably more AMPs were attached onto EDC/NHS activated ELP surfaces compared to non-activated surfaces, as shown in Figure 23. The same trend was observed on the activated and non-activated Ti surfaces. However, the AMP amount bound to Ti surfaces after EDC/NHS activation was significantly lower. Upon rinsing with Milli-Q water, most of the AMP remained on the activated ELP surface while the whole content of AMPs was released from the other surfaces. These results confirm a stable attachment of AMP onto ELP surfaces via the EDC/NHS coupling approach.

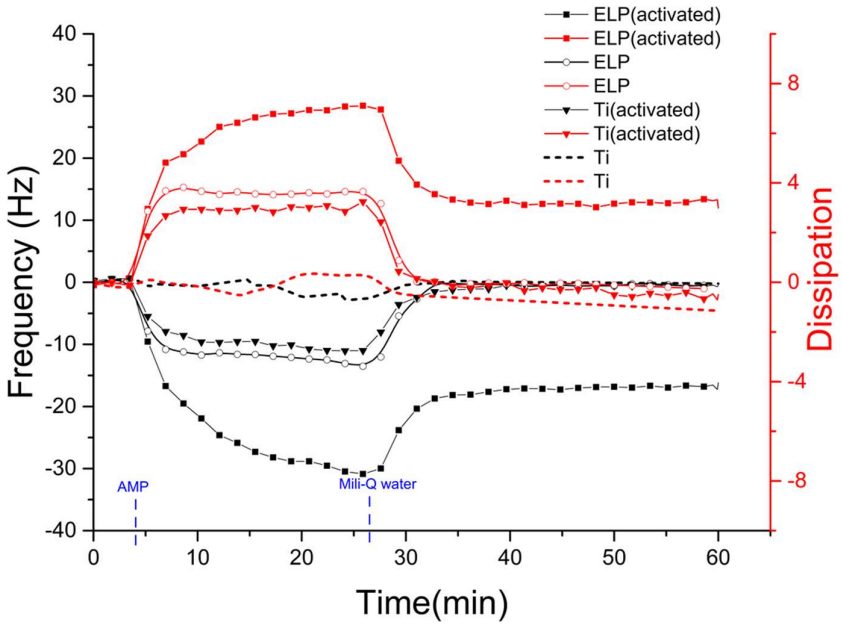

Figure 23. QCM-D results obtained from loading and washing AMP onto ELP surfaces with and without EDC-NHS activation. Pure Ti surfaces were used as control.

As a proof to show that covalently attached AMPs are not leached out from hydrogel substrates, a zone inhibition test was performed using *S. aureus*. A visible inhibition zone around hydrogels with physically loaded AMPs was detected as shown in Figure 24. Such zone is a result of bacterial eradication around the hydrogel due to release of physically bonded AMPs into the BHI agar plate surface. No inhibition zone was found around hydrogels with covalently bonded AMPs. Such property is very important to create contact killing surfaces to preserve their antibacterial effect for a longer time.

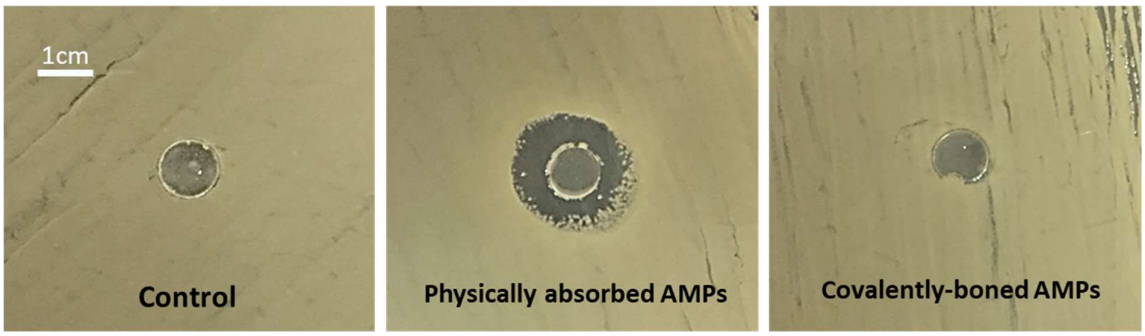

Figure 24. Images of the three different types of hydrogels when grown on BHI agar plate streaked with *S.aureus* in its log phase. From left to right is the hydrogel, the physically adsorbed AMP-hydrogel and lastly the covalently attached AMP-hydrogel.

6.2.2 Antibacterial performance of contact-killing surfaces

Both types of contact killing substrates developed in this thesis showed high antimicrobial efficacy against *S. epidermidis, S. aureus* and *P. aeruginosa*. Moreover, AMP-hydrogels even showed to be very effective towards two resistant strains of bacteria MRSA and MDR *E. coli*. The images of live and dead bacteria obtained by fluorescent microscopy shown in Figures 25 and 27, show a high population of dead cells on surfaces with covalently attached AMPs compared to the ones without AMP. The statistical data show significant increase in the dead population of bacteria, including the resistant types on AMP treated surfaces, Figure 26, 28 and 29.

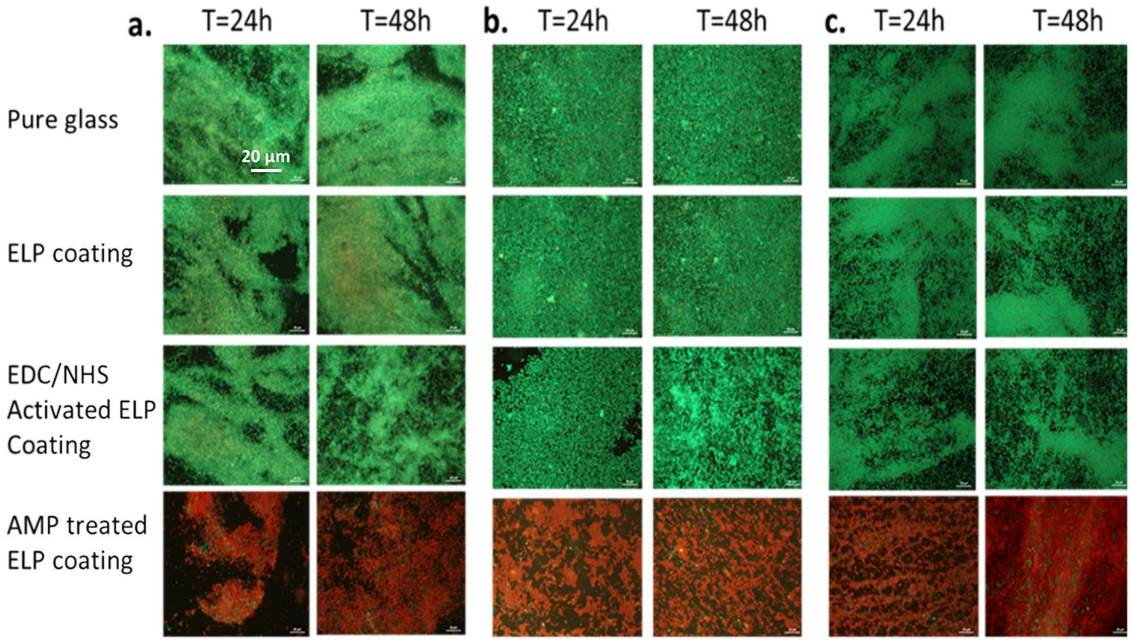

Figure 25. Images of biofilms formed onto ELP thin films with and without AMP. The bacteria are stained with SYTO® 9 and propidium iodide. The live bacteria appear green and the dead bacteria appear red. **a,** *S. epidermidis* **b,** *S. aureus* and **c,** *P. aeruginosa.*

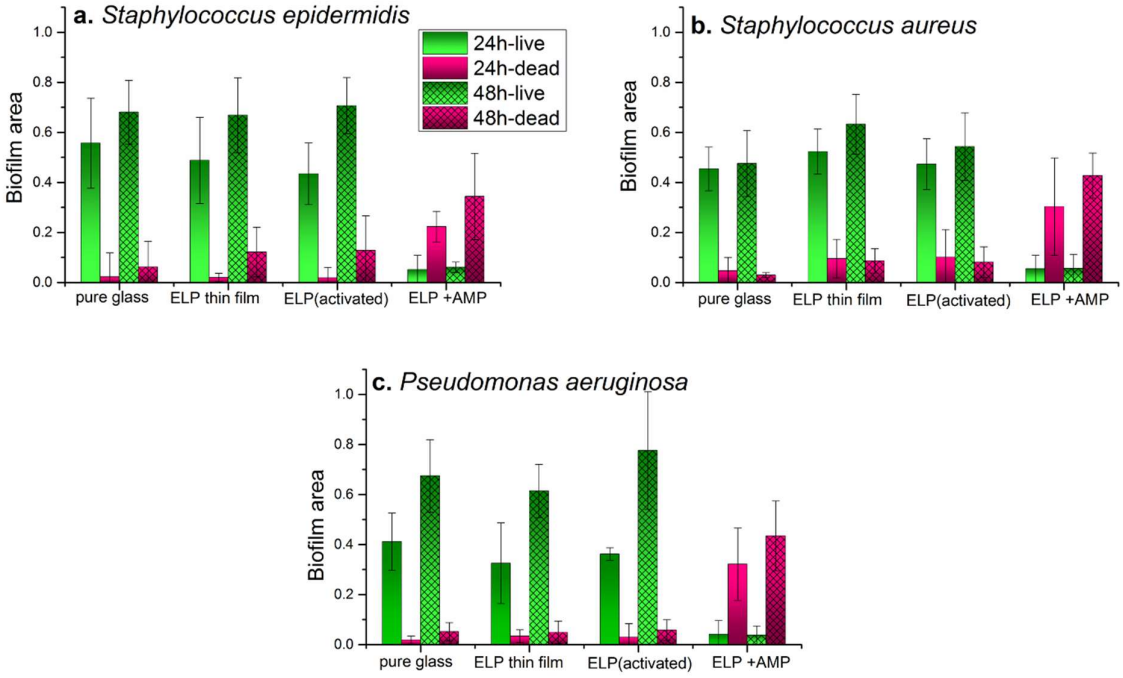

Figure 26. Data from analyzing the live and dead fractions of biofilms formed on ELP surfaces with and without AMP. The values are obtained from analyzing fluorescent images. Values are mean ±SD, N=3.

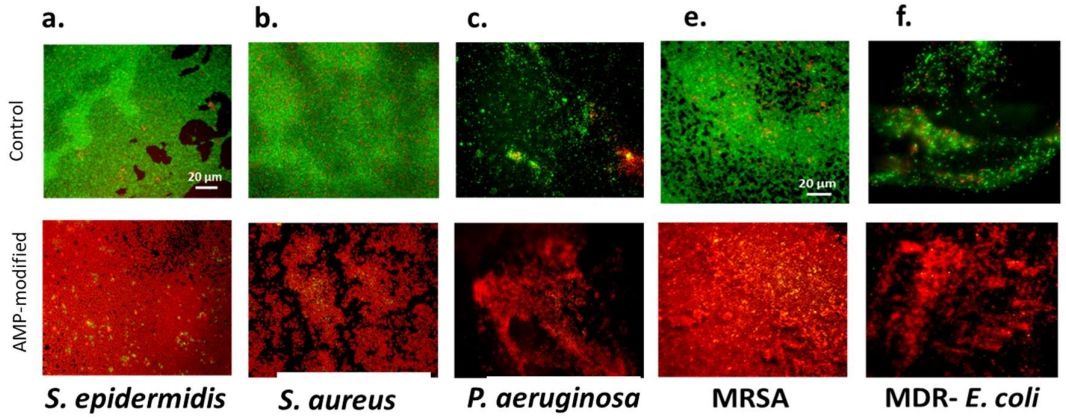

Figure 27. Images of biofilms formed onto AMP-hydrogels with and without AMP. The bacteria were stained by SYTO® 9 and propidium iodide. The live bacteria appear green and the dead bacteria appear red. **a,** *S. epidermidis* **b,** *S. aureus* and **c,** *P. aeruginosa* **e,** MRSA **f,** MDR *E. coli.*

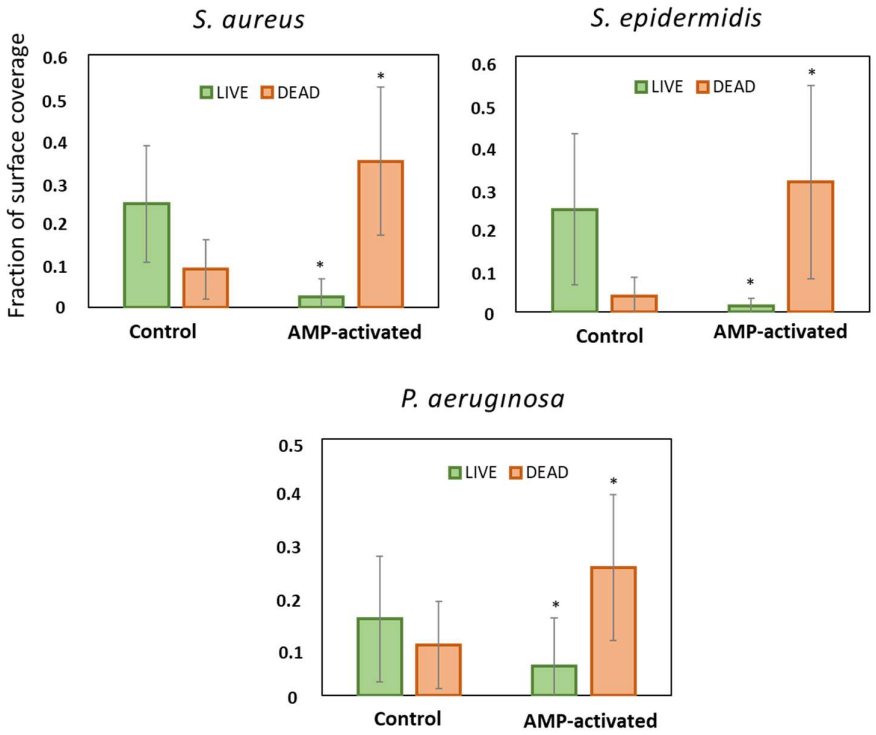

Figure 28. Data from analyzing the live and dead fractions of bacterial colonization on AMP-hydrogel surfaces with and without AMP attachment. The values are obtained from analyzing fluorescent images using ImageJ software. Values are mean ±SD, NC3, *p<0.05.

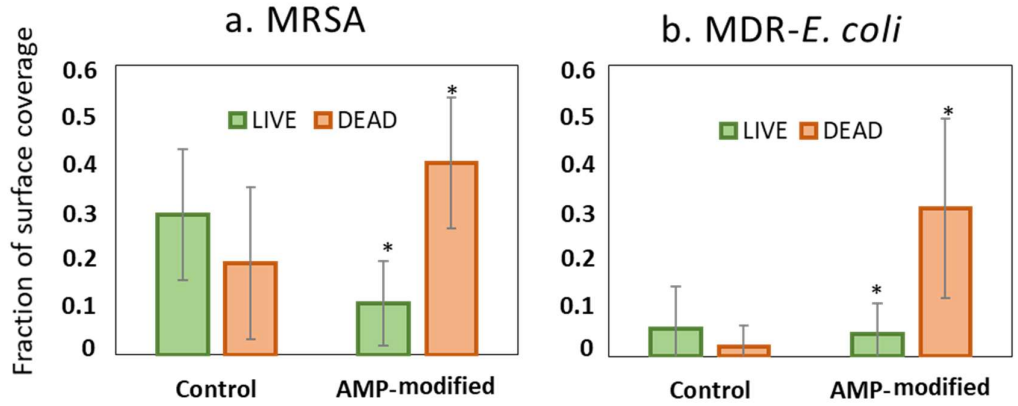

Figure 29. Data from analyzing the live and dead fractions of resistance bacteria a, MRSA and b, MDR-E. Coli formed on AMP-hydrogel surfaces with and without AMP attachment. The values are obtained from analyzing fluorescent images using Image J software. Values are mean ±SD, N=3, *p<0.05

The morphology of bacteria attached to AMP-elastin surfaces was evaluated using SEM and as shown in the micrographs in Figure 30, all types of bacteria underwent changes in their shapes and morphology when attached to AMP treated surfaces. The overall results imply that the interaction of AMP with the bacteria surface causes a physical deformation of bacteria that leads to their death.

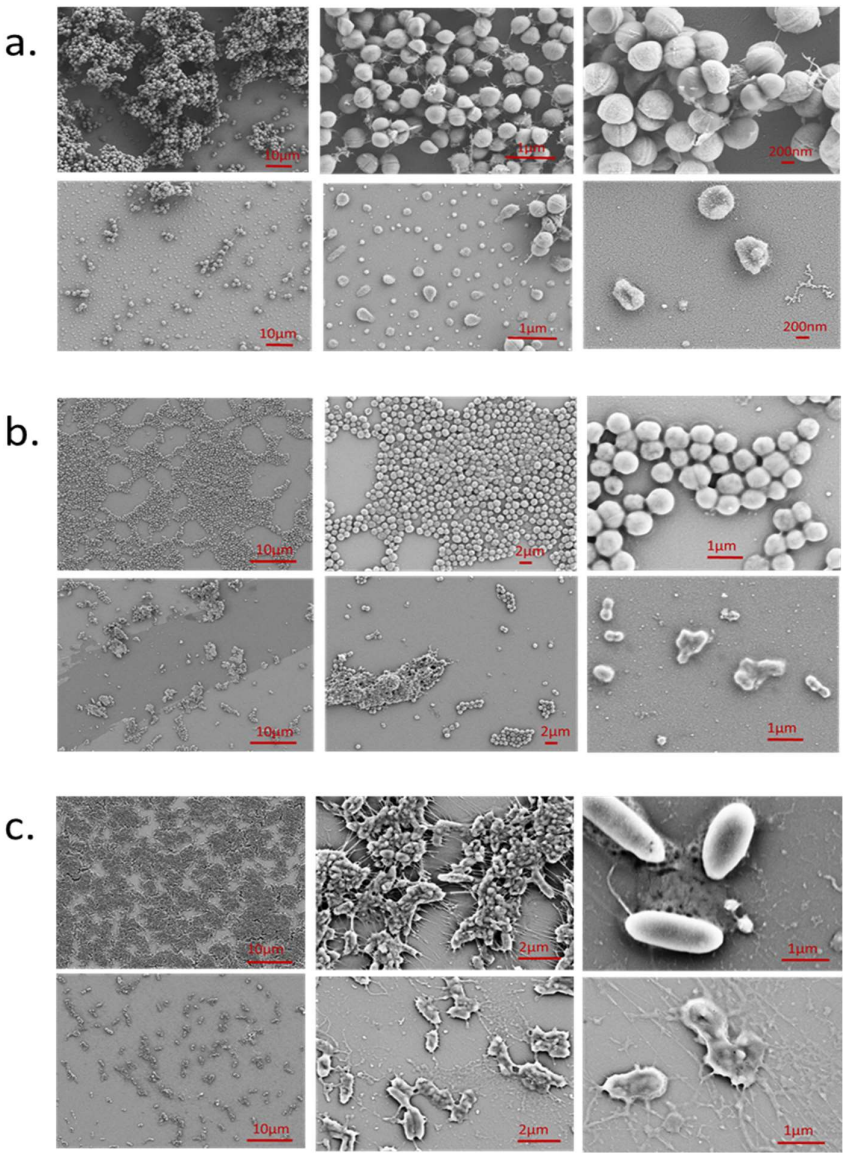

Figure 30. SEM images of bacteria taken after 24h **a,** *S. epidermidis* **b,** *S. aureus* and **c,** *P. aeruginosa.* The magnification increases from left to right. The pictures on the top row are the biofilms formed on ELP surfaces and the bottom row shows the bacteria grown on AMP functionalized ELP surfaces.

6.2.3 Assessment of stability of covalently attached peptides

One of the major obstacles to overcome in using AMPs clinically is their inherently low stability towards degradation.[54] This property can explain why AMPs that exhibit significant bacterial effect *in vitro*, do not act as effectively *in vivo*. Often high concentration of AMPs is used to compensate for their low *in vivo* activity which leads to an increase of their systemic cytotoxicity. To investigate whether covalent immobilization of peptides affect their half-life the stability of covalently bonded peptides in serum was investigated. This serum-based model was chosen since it has been reported that the *in vitro* stability in serum or plasma is a representative model for their *in vivo* bioavailability.[92] Fluorescently labelled peptides immobilized on ELP surfaces were seen to aggregate and detach from the surfaces after 24h when subjected to serum as shown in Figure 31. This is while the serum stability of the same analogues of peptides with short tryptophan and arginine rich sequences showed a half live of < 0.5h-6.5h.[92] The serum stability results corresponded well with bacterial assays where the AMP modified elastin substrates showed high bacterial killing effect up to 24h and the effect was lost at 48h (Figure 32). The loss of AMP activity in serum can be attributed to the presence of other proteins and enzymes in the serum. The peptides rich in cationic components are more susceptible to degradation since the charged components in their structure such as arginine and lysine content, expose a higher number of cleavage sites to degrading enzymes.[93]

Similar results were achieved for AMP-hydrogel surfaces. From the results of the bacterial assays shown in Figure 33, the peptides show high antibacterial activity against *S. aureus* for 48h. Considering an infection-preventive wound patch made of AMP-hydrogel, a 48h antibacterial activity can be enough to eradicate bacteria present in the wound during early process of wound healing.

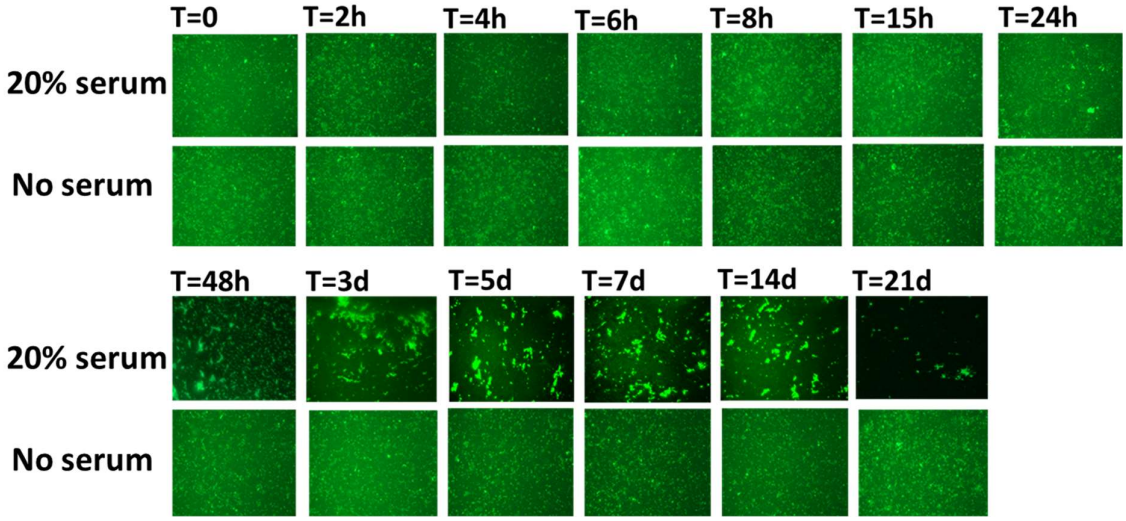

Figure 31. Fluorescence microscopy images of 5(6) Carboxyfluorescein tagged RRPRPRPRPWWWW-NH_2 immobilized onto ELP surfaces treated in 20% human blood serum at different duration of time. Milli-Q water treated peptides was used as control.
(S= 20% serum media, W= Milli-Q water media)

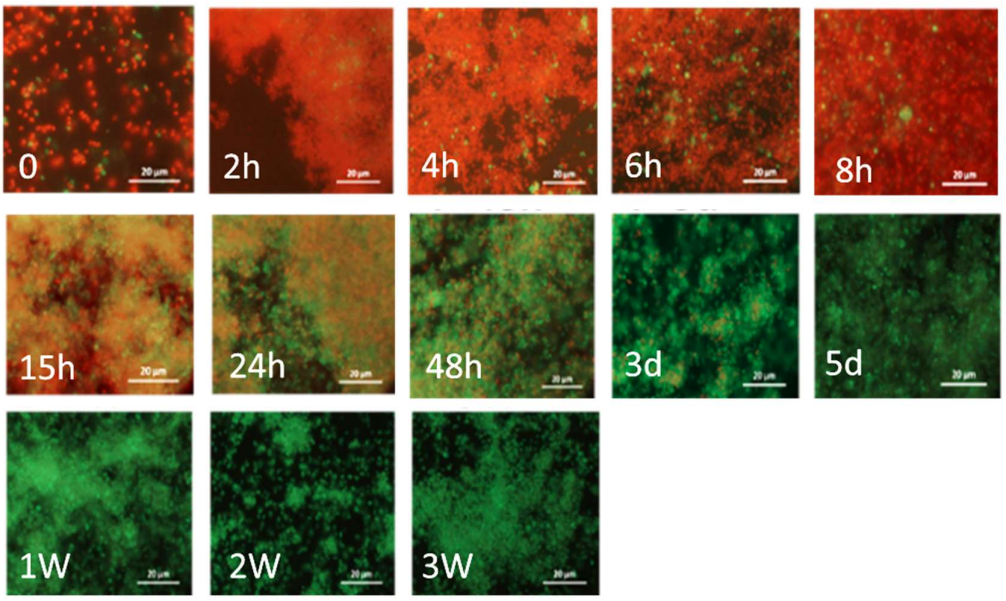

Figure 32. Bacteria (*S. epidermidis*) response to AMP functionalized surfaces treated in 20% serum at different duration of time.

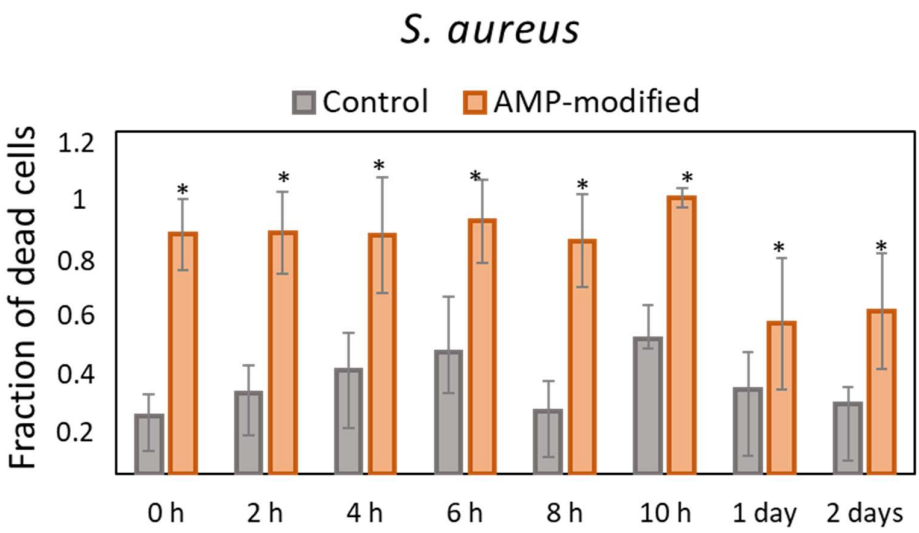

Figure 33. The proportion of dead cells (*S. aureus*) on hydrogel surfaces with and without AMP, incubated up to 2 days in 20% human serum. The data calculated by images from live/dead staining at each time point. Values are mean ±SD, N=3, *p<0.05.

6.2.4 *In vivo* and toxicity assessments

A pilot *in vivo* study was performed to acquire knowledge of the antibacterial activity and performance of AMP-hydrogels in a rat-model. Two dosages of bacterial inoculation (10^4 and $2x10^6$ CFU) were used and viability and CFU counting were obtained from retrieved implants and the exudates at two different time points (24h and 72h). The CFU results are presented in Figure 34, showing 10-100x higher numbers of CFUs from hydrogels without AMP compared to AMP-hydrogels for both inoculums at 24h and 72h. Although the difference was larger for 24h than for 72h. Over time, there was a clear increase in CFUs from AMP-hydrogel implants. This corresponds well to our previous *in vitro* experiments where a significant loss of AMP activity was found after 48h. Therefore, after 72h the AMPs might have lost some of their activity. CFUs from AMP-hydrogel exudates were not significantly different over time. However, the amount of CFU in exudates from hydrogels with and without AMP differed with different time points and inoculum sizes and did not follow any regular pattern. In the tests performed at 10^4 CFU dose, a decrease in CFU count was observed for 72h and for 10^6 CFU dose, the same behaviour occurred at 24h.

Overall, considering the results from retrieved hydrogels in pilot *in vivo* study, there was a clear decrease in the number of bacteria attached to AMP-hydrogels compared to those without AMPs. However, a more comprehensive *in vivo* study with a model that more closely resembles an infected wound is needed to confirm the efficacy of AMP-hydrogels.

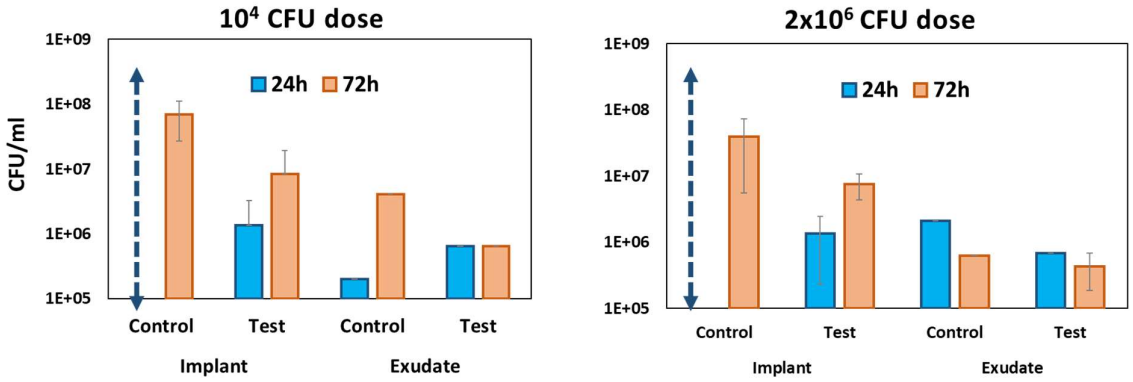

Figure 34. The amount of CFU adhering to the hydrogels and present in exudates at 24h and 72h inoculated with a, 10^4 and b, $2x10^6$ CFU dose. (Arrow: Not countable, but more than corresponding test disk and similar to same dilution at 72h)

The viability of human bone marrow-derived mesenchymal stem cells (hMSCs) on ELP surfaces modified by AMP immobilization was studied by live/dead imaging using fluorescent microscopy. There were no visible changes in the viability of the cells adhered to ELP surfaces after AMP immobilization (Figure 35). These data indicate that introducing AMPs onto ELP surfaces via covalent immobilization, did not disturb the cell-adhesivity to the substrates and showed no toxicity to the mammalian cells used.

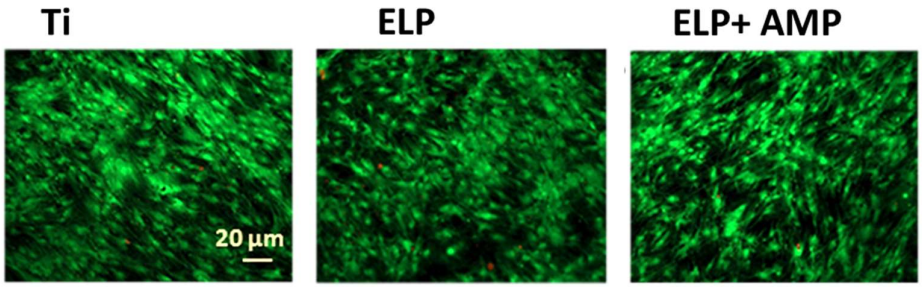

Figure 35. Live/Dead imaging of hMSCs cells on ELP surfaces coated on Ti discs with and without AMP modification. Cells are stained with calcein AM (live stain, green) and ethidium homodimer (dead stain, red).

Moreover, it was shown that the AMPs attached to hydrogel surfaces did not affect the viability of fibroblasts studied by MTT assays, Figure 36. The results suggest that while the presence of AMPs on the hydrogel introduced a high bacterial killing effect, it did not add any toxicity to human-derived cells used in this study (more than 70% cell viability). Such property makes the AMP-hydrogel a suitable selective antibacterial surface to be used for prevention of bacterial infection in wound management without harming host tissue cells.

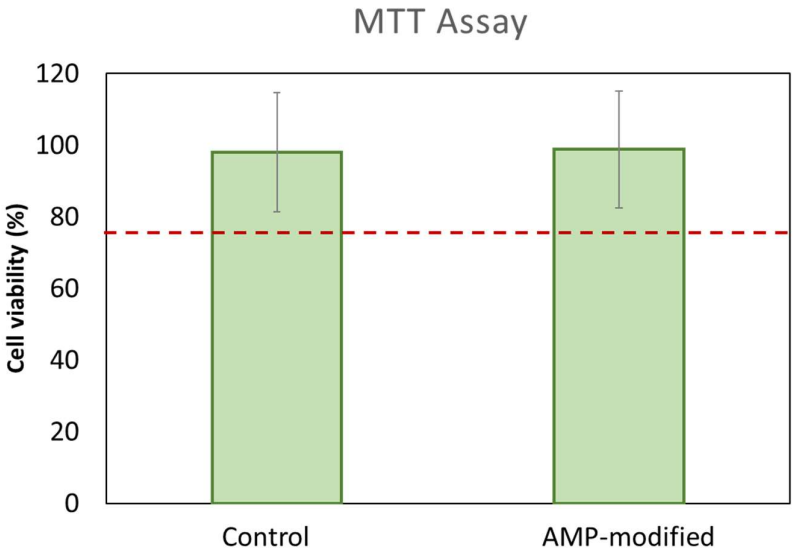

Figure 36. The cell viability obtained by two MTT assays performed on fibroblast with media exposed to control and test samples. The red line indicates 75% cell viability. Samples that are higher than this is regarded as non-toxic. The hydrogels analyzed were the control and the covalently attached AMPs, with 2x4 hydrogels each. Both different kind of samples showed a significantly higher cell viability than the 75% cut-off.

It has previously been shown that ELP coatings can promote mineralization of hMSCs on Ti surfaces.[64] To assess if AMP modification can affect the early-stage osteogenic differentiation of hMSCs on ELP-coated substrates, alkaline phosphatase (ALP) activity was quantified. The results shown in Figure 37a, imply that the presence of AMPs on ELP surfaces does not interfere with the early onset of ELP-induced differentiation of hMSCs.

Calcium deposition, which is known to occur after ALP activation, showed no statistically significant differences across all surfaces tested. Both AMP-treated surfaces showed similar calcium deposition to non-treated ELP and bare titanium surfaces, hence the mineralization on the surfaces was not affected by the presence of AMPs (Figure 37b). The overall conclusion is that AMP modification does not interfere with the osseointegrative properties of ELP-coated surfaces over 28 days *in vitro*.

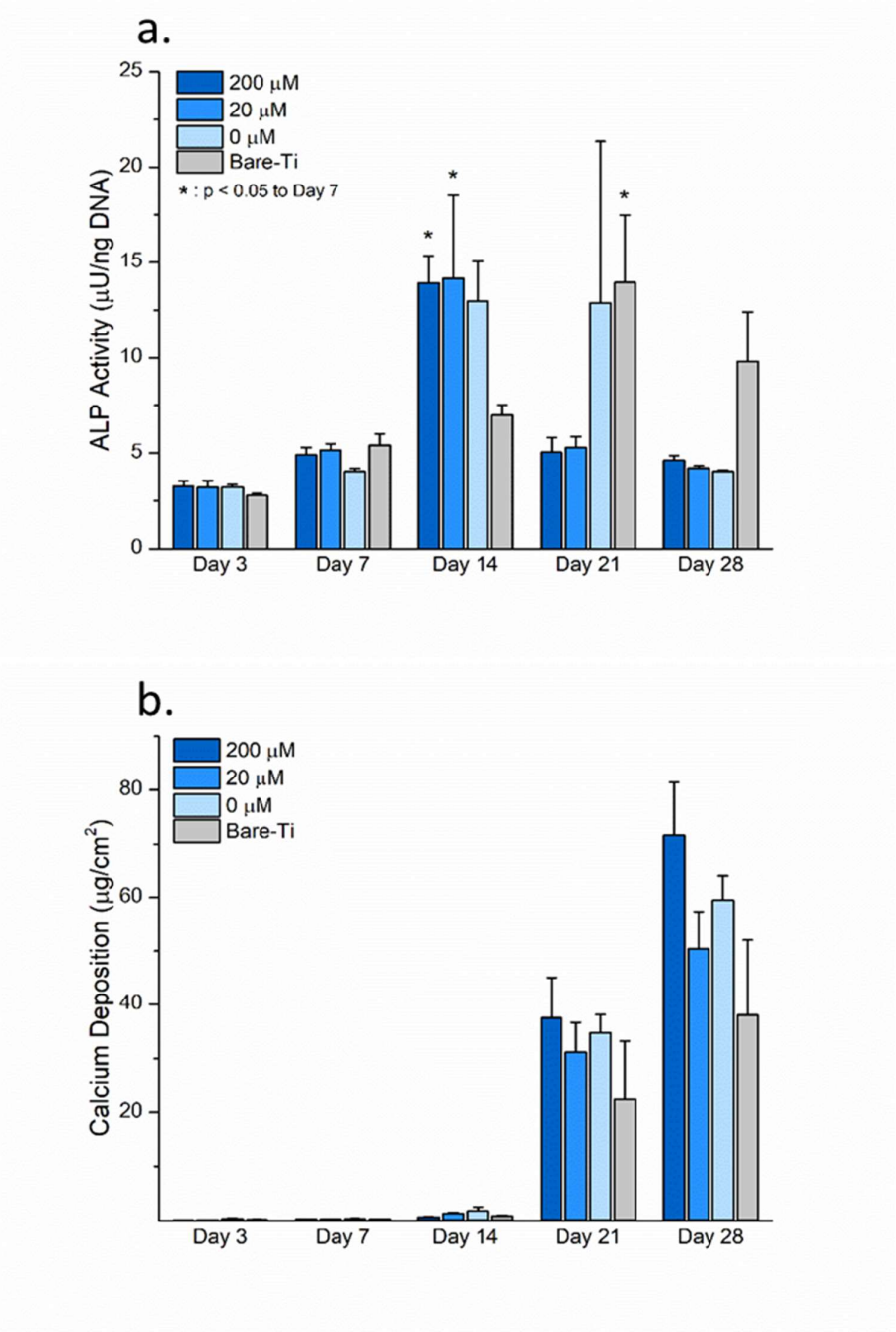

Figure 37. a, ALP activity of hMSCs seeded onto bare Ti or ELP substrates with 0, 20, or 200 μM of AMP. ALP activity is normalized to DNA concentration. **b,** Total calcium deposition of hMSCs seeded onto substrates. Values are mean ±SD, $^{*}p<0.05$.

For a proper wound management, the control of bleeding is a vital factor that involves the formation of a fibrin clot in the wound in which platelets are trapped and release inflammatory chemokines to initiate the healing processes.[94] That stage will create lateral responses to activate inflammatory responses and subsequent wound healing.[95] Therefore we investigated how the presence of AMPs in the hydrogels can affect the blood coagulation. Fresh whole blood from 2 different donors were used in the experiments, where the number of platelets were quantified before and after 1h of exposure to the hydrogels. A clearly visible clot formation was observed onto AMP-hydrogel compared to the ones without AMP, shown in Figure 37b. As expected from the observations, the results from platelet counting (shown in Figure 38a) showed significantly lower number of platelets in the presence of AMPs. The results suggest that using AMP-hydrogel as a wound patch can accelerate blood coagulation and clot formation on a bleeding wound. This can be considered as a desired additional property introduced by AMP-hydrogels apart from the superior antibacterial effect.

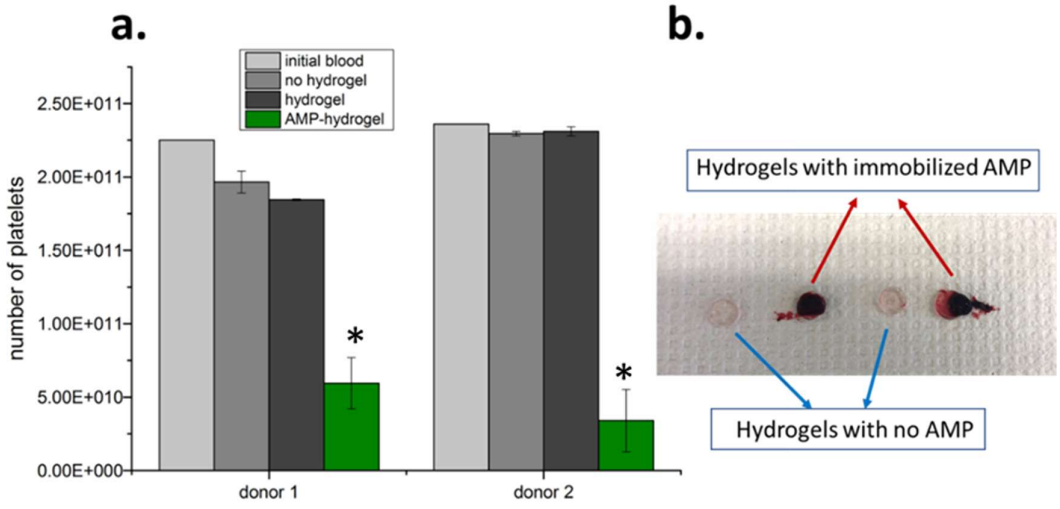

Figure 38. a, number of platelets after whole blood incubation at 37° for 60 min. Data represents mean ±SD, N=4, *p<0.05 and **b,** photo from appearance of the hydrogels after 1h blood contact.

7 Conclusions

Antibacterial surfaces are promising solutions for early prevention of biomaterial associated infection and to decrease the bioburden in a contaminated wound post-surgery.

In this thesis, the design and performance of two categories of antibacterial surfaces were introduced and discussed. We developed an antibiotic releasing substrate using mesoporous titania thin films. MPT thin films with pore sizes of 4, 6 and 7 nm were successfully synthesised and loaded with antibiotics. Antimicrobial behaviour of all surfaces was improved by antibacterial loading and the effect correlated well with the amount of antibiotic released from each substrate. By combining with an additional thin film made of a thermo-responsive polymer (PNIPAAm) with incorporated gold nanorods, we created a photon-induced drug-delivery coating that could induce the initial drug release using NIR irradiation and observed a desired property in inhibition of bacterial growth.

In a separate approach, we fabricated and evaluated contact killing surface coatings. AMPs were successfully immobilized onto ELP and F127 hydrogel substrates using EDC-NHS chemistry and the functionalized surfaces showed high bacterial killing efficacy against various strains of bacteria including resistant types as well as no toxicity to human-derived cells. Stability of covalent immobilized AMPs was shown to be improved compared to AMPs in free state.

The work that has been performed and presented in this thesis, suggest useful strategies for development of antibacterial coatings for biomedical applications with an aim to decrease overall usage of antibiotic for treatment and prevention of BAI and post implantation surgery wounds. The hope is that these approaches can be shaped and adapted further for designing functional antibacterial medical devices and implants to bring practical benefits for patients in need and most importantly help to fight antibiotic resistance worldwide.

8 *Acknowledgements*

Undertaking my doctoral research at Applied Chemistry at Chalmers University of Technology has truly been a life-changing experience for me. Along the way, I realized that the real purpose of research, is to see a bigger picture rather than only accomplishing a project. I enjoyed working with every bit of my research, at liberty, exploring new ideas and embracing it as an important part of my life. In this journey, I had the fortune of being surrounded by many individuals to whom I owe my gratitude;

Thanks to **Knut and Alice Wallenberg foundation** and the **Area of Advanced Materials Science** at Chalmers university of technology for financing my project.

Special thanks to my supervisor, Professor **Martin Andersson**. It was a pleasure to work under your guidance throughout the past years. Thanks for being so considerate as a mentor, for all the valuable knowledge you shared with me, providing your professional support at all stages of my PhD project - letting me enjoy the science to the fullest. Looking back at the personal development and the path of my potential career, I cannot thank you enough for your direct involvement and your immense source of motivation.

My examiner, professor **Anders Palmqvist**, thank you for all your support during my time as a PhD student. It was a pleasure to work with you.

My co-supervisor, co-author and officemate, Dr. **Mats Hulander**. You have been an important part of my PhD journey and made it double joyful for me. Your feedback on this thesis has been beyond valuable. Thank you for all the energy, motivations, good talks and all the unforgettable memories we shared past years. Thanks for being there every time I needed your professional and personal help.

Professor **Thomas Webster** for giving me the opportunity to visit your lab at Northeastern University and co-work with your wonderful lab members: **Erik Taylor**, **Batur Ercan** and **Stanley Chung.**

Professor **Sarah Heilshorn**, having the pleasure to collaborate with your lab group at Stanford University, was a brilliant experience and I learnt so much during those months. Thank you, **Chris Lindsay**, for welcoming me and helping me in the lab during my visit.

Hanna Härelind, my former director of doctoral studies and new head of the division. You are an inspiring woman and thanks for all the effort you put into making our division a pleasant place to work.

Associate professor **Jaan Hong**, thanks for helping with blood tests in paper IV, **Anne Wendel** for helping with XPS results and **Maxlab** at Lund for assisting with SAXS measurements.

Former and new MA research group members, **Maria Pihl** (thanks for getting me introduced to "microbiology lab" and being a great collaborator, co-author and friend), **Johan Karlsson** (you were the best supervisor during my master thesis project), **Andy Lotsari** (thanks for all the girl talks and chocolates we had together!), **Simon Isaksson** (for all the fun time with innebandy, office pranks and making ice cream with liquid nitrogen!), **Edvin Blomstrand** (thanks for all your dedication on our research and I am so excited to work with you in the future), **Astrid**, **Gustav, Annija** and **Joyce.**

Dr. Anand Kumar, we grew as individuals at MA research group and joined forces into starting "our dream start-up". Cannot wait to join you and see where it will take us and where we will take it.

Giulio and **Milene**, your friendship is a gift I will always treasure. You are the family I chose to have. Thanks for being there at any time I needed you.

My amazing friends **Johanna**, **Ting** and **Simone**. Thanks for all the unforgettable memories we share and many more to come.

All the great colleagues/friends at **TYK** and **KCK**, **Gunnar**, **Sam**, **Peter**, **Carl-Robert, Anna** and many others. You all made me "love to go to work" every day. Thanks for all the help, laughs, cakes, talks and parties.

My mom and dad, your unconditional love is what I grew up with. I know how hard it was for you to raise your kids in a country where all the rules were against your values. Thanks for putting effort into shaping me into a free and happy woman despite all the limitations we faced. I am proud to call you my parents.

My siblings **Nasim and Ali**. You are the meaning of my life. I looked up to you since the day I started knowing myself. I am grateful for having the chance to grow up by your side. Thanks for my amazing nephews **Kasra** and **Parsa** and my gorgeous sister in law **Farinaz**.

Farzi and Kamran, my parents in law and best grandparents to my son, thank you for supporting our little family.

Ryan, the shining star of my life. If you ever look at this thesis, I hope you will be proud of mommy who wrote it with an energetic toddler around her. Always remember that no one could change me as much as you did, and I am so grateful for that.

My husband and my best friend, **Mehregan Redjamand,** for being a constant source of support and love. You always believe in me even in my weakest moments and see the awesomeness in me even at times I am a mess. Your love and support is the reason why I dare to dream big. With you by my side, I am the strongest.

9. REFERENCES

1. Meng, E. & Sheybani, R. Insight: Implantable medical devices. *Lab Chip* **14**, 3233–3240 (2014).
2. Hetrick, E. M. & Schoenfisch, M. H. Reducing implant-related infections: Active release strategies. *Chem. Soc. Rev.* **35**, 780–789 (2006).
3. Zaborowska, M. *et al.* Bacteria-material surface interactions: Methodological development for the assessment of implant surface induced antibacterial effects. *J. Biomed. Mater. Res. - Part B Appl. Biomater.* **103**, 179–187 (2015).
4. Riool, M. *et al.* Staphylococcus epidermidis originating from titanium implants infects surrounding tissue and immune cells. *Acta Biomater.* **10**, 5202–5212 (2014).
5. Wysocki, A. B. Evaluating and managing open skin wounds: colonization versus infection. *AACN Clin. Issues* **13**, 382–397 (2002).
6. Went, P. & Martin, B. F. RECURRENCE OF INFECTION AFTER REVISION OF performed. 307–309
7. Costerton, J. W. Bacterial Biofilms: A Common Cause of Persistent Infections. *Science (80-.).* **284**, 1318–1322 (1999).
8. Roy, R., Tiwari, M., Donelli, G. & Tiwari, V. Strategies for combating bacterial biofilms: A focus on anti-biofilm agents and their mechanisms of action. *Virulence* **9**, 522–554 (2018).
9. Woodford, N. & Livermore, D. M. Infections caused by Gram-positive bacteria: a review of the global challenge. *J. Infect.* **59**, S4–S16 (2009).
10. Alanis, A. J. Resistance to antibiotics: Are we in the post-antibiotic era? *Arch. Med. Res.* **36**, 697–705 (2005).
11. Storr, J. *et al.* Core components for effective infection prevention and control programmes: New WHO evidence-based recommendations. *Antimicrob. Resist. Infect. Control* **6**, (2017).
12. Hasan, J., Crawford, R. J. & Ivanova, E. P. Antibacterial surfaces: The quest for a new generation of biomaterials. *Trends Biotechnol.* **31**, 295–304 (2013).
13. Matl, F. D. *et al.* New Anti-Infective Coatings of Medical Implants New Anti-Infective Coatings of Medical Implants □. (2008). doi:10.1128/AAC.01438-07
14. Gao, W., Chen, Y., Zhang, Y., Zhang, Q. & Zhang, L. Nanoparticle-based local antimicrobial drug delivery ☆. *Adv. Drug Deliv. Rev.* **127**, 46–57 (2018).
15. Karlsson, J. *et al.* Localized Controlled Drug Delivery from Mesoporous Implants Dept . Chemical and Biological Engineering , Chalmers University of Technology , Kemivägen 10 , In Vitro Apatite formation 2 MATERIALS AND METHODS Material Preperation In Vitro Drug Adsorption an. **2**, 250–253 (2014).
16. Liu, Y. *et al.* Nanotechnology-based antimicrobials and delivery systems for biofilm-infection control. *Chem. Soc. Rev.* **48**, 428–446 (2019).

17. Luo, Z. *et al.* Biomaterials Intracellular redox-activated anticancer drug delivery by functionalized hollow mesoporous silica nanoreservoirs with tumor speci fi city. *Biomaterials* **35**, 7951–7962 (2014).

18. Wang, S. Ordered mesoporous materials for drug delivery. *Microporous Mesoporous Mater.* **117**, 1–9 (2009).

19. Vivero-escoto, J. L., Chiang, Y., Wu, K. C. & Yamauchi, Y. Recent progress in mesoporous titania materials : adjusting morphology for innovative applications. **13**, (2012).

20. Zhang, R., Elzatahry, A. A., Al-deyab, S. S. & Zhao, D. Mesoporous titania : From synthesis to application. *Nano Today* **7**, 344–366 (2012).

21. Wu, K. C., Yamauchi, Y., Hong, C., Yang, Y. & Liang, Y. ChemComm for intracellular imaging and anticancer drug delivery w. 5232–5234 (2011). doi:10.1039/c1cc10659g

22. Mcmaster, W. A., Wang, X. & Caruso, R. A. Collagen-Templated Bioactive Titanium Dioxide Porous Networks for Drug Delivery. (2012). doi:10.1021/am301093k

23. Karlsson, J., Harmankaya, N., Tengvall, P. & Andersson, M. Ex vivo alendronate localization at the mesoporous titania implant / bone interface. (2015). doi:10.1007/s10856-014-5337-7

24. Karlsson, J. Controlling drug delivery kinetics from mesoporous titania thin films by pore size and surface energy. 4425–4436 (2015).

25. Xia, W., Grandfield, K., Hoess, A., Ballo, A. & Cai, Y. Mesoporous titanium dioxide coating for metallic implants. doi:10.1002/jbm.b.31925

26. Woong, S. *et al.* Applied Surface Science Mesoporous TiO 2 implants for loading high dosage of antibacterial agent. *Appl. Surf. Sci.* **303**, 140–146 (2014).

27. Gulati, K. *et al.* Biocompatible polymer coating of titania nanotube arrays for improved drug elution and osteoblast adhesion. *Acta Biomater.* **8**, 449–456 (2012).

28. Liu, F. & Urban, M. W. Recent advances and challenges in designing stimuli-responsive polymers. *Prog. Polym. Sci.* **35**, 3–23 (2010).

29. Jeong, B., Kim, S. W. & Bae, Y. H. Thermosensitive sol-gel reversible hydrogels. *Adv. Drug Deliv. Rev.* **54**, 37–51 (2002).

30. Kavanagh, C. A., Rochev, Y. A., Gallagher, W. M., Dawson, K. A. & Keenan, A. K. Local drug delivery in restenosis injury: Thermoresponsive co-polymers as potential drug delivery systems. *Pharmacol. Ther.* **102**, 1–15 (2004).

31. Pişkin, E., Dinçer, S. & Türk, M. Gene delivery: Intelligent but just at the beginning. *J. Biomater. Sci. Polym. Ed.* **15**, 1181–1202 (2004).

32. Karg, M., Pastoriza-Santos, I., Pérez-Juste, J., Hellweg, T. & Liz-Marzán, L. M. Nanorod-coated PNIPAM microgels: Thermoresponsive optical properties. *Small* **3**, 1222–1229 (2007).

33. Alkilany, A. M., Thompson, L. B., Boulos, S. P., Sisco, P. N. & Murphy, C. J. Gold nanorods: Their potential for photothermal therapeutics and drug delivery, tempered by the complexity of their biological interactions. *Adv. Drug Deliv. Rev.* **64**, 190–199 (2012).

34. Gorelikov, I., Field, L. M. & Kumacheva, E. Hybrid microgels photoresponsive in the near-infrared spectral range. *J. Am. Chem. Soc.* **126**, 15938–15939 (2004).

35. Kawano, T., Niidome, Y., Mori, T., Katayama, Y. & Niidome, T. PNIPAM gel-coated gold nanorods for targeted delivery responding to a near-infrared laser. *Bioconjug. Chem.* **20**, 209–212 (2009).

36. Shiotani, A., Mori, T., Niidome, T., Niidome, Y. & Katayama, Y. Stable incorporation of gold nanorods into N-isopropylacrylamide hydrogels and their rapid shrinkage induced by near-infrared laser irradiation. *Langmuir* **23**, 4012–4018 (2007).

37. Das, M., Sanson, N., Fava, D. & Kumacheva, E. Microgels loaded with gold nanorods: Photothermally triggered volume transitions under physiological conditions. *Langmuir* **23**, 196–201 (2007).

38. Adlhart, C. *et al.* Surface modifications for antimicrobial effects in the healthcare setting: a critical overview. *J. Hosp. Infect.* **99**, 239–249 (2018).

39. Kaur, R. & Liu, S. Antibacterial surface design – Contact kill. *Prog. Surf. Sci.* **91**, 136–153 (2016).

40. Ghanbar, S., Kazemian, M. R. & Liu, S. New Generation of N-Chloramine/QAC Composite Biocides: Efficient Antimicrobial Agents to Target Antibiotic-Resistant Bacteria in the Presence of Organic Load. *ACS Omega* **3**, 9699–9709 (2018).

41. He, W. *et al.* A Novel Surface Structure Consisting of Contact-active Antibacterial Upper-layer and Antifouling Sub-layer Derived from Gemini Quaternary Ammonium Salt Polyurethanes. *Sci. Rep.* **6**, 1–9 (2016).

42. Bahar, A. A. & Ren, D. Antimicrobial peptides. *Pharmaceuticals* **6**, 1543–1575 (2013).

43. Ohtani, K., Okada, T., Yoshizumi, H. & Kagamiyama, H. Complete primary structures of two subunits of purothionin A, a lethal protein for brewer's yeast from wheat flour. *J. Biochem.* **82**, 753–767 (1977).

44. HIRSCH, J. G. Phagocytin: a bactericidal substance from polymorphonuclear leucocytes. *J. Exp. Med.* **103**, 589–611 (1956).

45. Law Whyte, L. *et al.* Organisms. *Universe Exp.* **415**, 63–74 (2018).

46. Hancock, R. E. W. & Scott, M. G. The role of antimicrobial peptides in animal defenses. *Proc. Natl. Acad. Sci. U. S. A.* **97**, 8856–8861 (2000).

47. Loppnow, H. *et al.* Cytokine induction by lipopolysaccharide (LPS) corresponds to lethal toxicity and is inhibited by nontoxic Rhodobacter capsulatus LPS. *Infect. Immun.* **58**, 3743–3750 (1990).

48. Huang, H. W. Molecular mechanism of antimicrobial peptides: The origin of cooperativity. *Biochim. Biophys. Acta - Biomembr.* **1758**, 1292–1302 (2006).

49. Nizet, V. Antimicrobial peptide resistance mechanisms of human bacterial pathogens. *Curr. Issues Mol. Biol.* **8**, 11–26 (2006).

50. Loeffler, J. M., Nelson, D. & Fischetti, V. A. Rapid killing of Streptococcus pneumoniae with a bacteriophage cell wall hydrolase. *Science (80-.).* **294**, 2170–2172 (2001).

51. Ding, X. *et al.* NIH Public Access. **16**, 387–393 (2013).

52. Yeaman, M. R. & Yount, N. Y. Mechanisms of antimicrobial peptide action and resistance. *Pharmacol. Rev.* **55**, 27–55 (2003).

53. Pasupuleti, M., Schmidtchen, A., Chalupka, A., Ringstad, L. & Malmsten, M. End-tagging of ultra-short antimicrobial peptides by W/F stretches to facilitate bacterial killing. *PLoS One* **4**, (2009).

54. Svenson, J. *et al.* Antimicrobial peptides with stability toward tryptic degradation. *Biochemistry* **47**, 3777–3788 (2008).

55. Costa, F., Carvalho, I. F., Montelaro, R. C., Gomes, P. & Martins, M. C. L. Covalent immobilization of antimicrobial peptides (AMPs) onto biomaterial surfaces. *Acta Biomater.* **7**, 1431–1440 (2011).

56. Haynie, S. L., Crum, G. A. & Doele, B. A. Antimicrobial activities of amphiphilic peptides covalently bonded to a water-insoluble resin. *Antimicrob. Agents Chemother.* **39**, 301–307 (1995).

57. Willcox, M. D. P., Hume, E. B. H., Aliwarga, Y., Kumar, N. & Cole, N. A novel cationic-peptide coating for the prevention of microbial colonization on contact lenses. *J. Appl. Microbiol.* **105**, 1817–1825 (2008).

58. Batista, M. K. S., Gallemí, M., Adeva, A., Gomes, C. A. R. & Gomes, P. Facile regioselective synthesis of a novel chitosan-pexiganan conjugate with potential interest for the treatment of infected skin lesions. *Synth. Commun.* **39**, 1228–1240 (2009).

59. Bagheri, M., Beyermann, M. & Dathe, M. Immobilization reduces the activity of surface-bound cationic antimicrobial peptides with no influence upon the activity spectrum. *Antimicrob. Agents Chemother.* **53**, 1132–1141 (2009).

60. Gallardo-Moreno, A. M. *et al.* In vitro biocompatibility and bacterial adhesion of physico-chemically modified Ti6Al4V surface by means of UV irradiation. *Acta Biomater.* **5**, 181–192 (2009).

61. MacEwan, S. R. & Chilkoti, A. Elastin-like polypeptides: biomedical applications of tunable biopolymers. *Biopolymers* **94**, 60–77 (2010).

62. Cai, L. & Heilshorn, S. C. Designing ECM-mimetic materials using protein engineering. *Acta Biomater.* **10**, 1751–1760 (2014).

63. Raphel, J., Parisi-Amon, A. & Heilshorn, S. C. Photoreactive elastin-like proteins for use as versatile bioactive materials and surface coatings. *J. Mater. Chem.* **22**, 19429–19437 (2012).

64. Raphel, J. *et al.* Engineered protein coatings to improve the osseointegration of dental and orthopaedic implants. *Biomaterials* **83**, 269–282 (2016).

65. Bellis, S. L. Advantages of RGD peptides for directing cell association with biomaterials. *Biomaterials* **32**, 4205–4210 (2011).

66. Type, M. Surfactant Self-Assembly : Beyond the Spherical Micelle. (2014).

67. Alexandridis, P. & Alan Hatton, T. Poly(ethylene oxide)poly(propylene oxide)poly(ethylene oxide) block copolymer surfactants in aqueous solutions and at interfaces: thermodynamics, structure, dynamics, and modeling. *Colloids Surfaces A Physicochem. Eng. Asp.* **96**, 1–46 (1995).

68. Alexandridis, P. Amphiphilic copolymers and their applications. *Curr. Opin. Colloid Interface Sci.* **1**, 490–501 (1996).

69. Kaneko, T., Nagasawa, H., Gong, J. P. & Osada, Y. Liquid crystalline hydrogels: Mesomorphic behavior of amphiphilic polyacrylates bearing cholesterol mesogen. *Macromolecules* **37**, 187–191 (2004).

70. He, W. X., Rajasekharan, A. K., Tehrani-Bagha, A. R. & Andersson, M. Mesoscopically Ordered Bone-Mimetic Nanocomposites. *Adv. Mater.* **27**, 2260–2264 (2015).

71. Holmqvist, P., Alexandridis, P. & Lindman, B. Modification of the microstructure in block copolymer-water-"oil" systems by varying the copolymer composition and the 'oil' type: Small-angle X-ray scattering and deuterium-NMR investigation. *J. Phys. Chem. B* **102**, 1149–1158 (1998).

72. Selig, H. F. *et al.* The properties of an 'ideal' burn wound dressing - What do we need in daily clinical practice? Results of a worldwide online survey among burn care specialists. *Burns* **38**, 960–966 (2012).

73. Andreu, V., Mendoza, G., Arruebo, M. & Irusta, S. Smart dressings based on nanostructured fibers containing natural origin antimicrobial, anti-inflammatory, and regenerative compounds. *Materials (Basel).* **8**, 5154–5193 (2015).

74. Jayakumar, R., Prabaharan, M., Sudheesh Kumar, P. T., Nair, S. V. & Tamura, H. Biomaterials based on chitin and chitosan in wound dressing applications. *Biotechnol. Adv.* **29**, 322–337 (2011).

75. Niidome, T. *et al.* PEG-modified gold nanorods with a stealth character for in vivo applications. *J. Control. Release* **114**, 343–347 (2006).

76. Rajasekharan, A. K. & Andersson, M. Role of nanoscale confinement on calcium phosphate formation at high supersaturation. *Cryst. Growth Des.* **15**, 2775–2780 (2015).

77. Sharma, U., Pal, D. & Prasad, R. Alkaline phosphatase: An overview. *Indian J. Clin. Biochem.* **29**, 269–278 (2014).

78. Andersson, M. *et al.* Ag/AgCl-loaded ordered mesoporous anatase for photocatalysis. *Chem. Mater.* **17**, 1409–1415 (2005).

79. Weissleder, R. N EWS AND V IEWS A clearer vision for in vivo imaging Progress continues in the development of smaller , more penetrable probes for biological imaging . Toward the phosphoproteome. *1 Wet Chem. Synth. High Asp. Ratio Cylind. Gold Nanorods.pdf* (2001).

80. Li, X. *et al.* Antimicrobial functionalization of silicone surfaces with engineered short peptides having broad spectrum antimicrobial and salt-resistant properties. *Acta Biomater.* **10**, 258–266 (2014).

81. Chen, R. *et al.* Synthesis, characterization and in vitro activity of a surface-attached antimicrobial cationic peptide. *Biofouling* **25**, 517–524 (2009).

82. Humblot, V. *et al.* The antibacterial activity of Magainin I immobilized onto mixed thiols Self-Assembled Monolayers. *Biomaterials* **30**, 3503–12 (2009).

83. Costa, F., Carvalho, I. F., Montelaro, R. C., Gomes, P. & Martins, M. C. L. Covalent immobilization of antimicrobial peptides (AMPs) onto biomaterial surfaces. *Acta Biomater.* **7**, 1431–1440 (2011).

84. Yan, Q., Zheng, H. N., Jiang, C., Li, K. & Xiao, S. J. EDC/NHS activation mechanism of polymethacrylic acid: Anhydride versus NHS-ester. *RSC Adv.* **5**, 69939–69947 (2015).

85. Gupta, B., Agarwal, R. & Alam, M. S. Hydrogels for wound healing applications. *Biomed. Hydrogels* 184–227 (2011). doi:10.1533/9780857091383.2.184

86. Gupta, A. *et al.* The production and application of hydrogels for wound management: A review. *Eur. Polym. J.* **111**, 134–151 (2019).

87. Boge, L. *et al.* Cubosomes post-loaded with antimicrobial peptides: Characterization, bactericidal effect and proteolytic stability. *Int. J. Pharm.* **526**, 400–412 (2017).

88. Rajasekharan, A. K., Bordes, R., Sandström, C., Ekh, M. & Andersson, M. Hierarchical and Heterogeneous Bioinspired Composites—Merging Molecular Self-Assembly with Additive Manufacturing. *Small* **13**, 1–11 (2017).

89. Schibli, D. J., Hwang, P. M. & Vogel, H. J. The structure of the antimicrobial active center of lactoferricin B bound to sodium dodecyl sulfate micelles. *FEBS Lett.* **446**, 213–217 (1999).

90. Jing, W., Hunter, H. N., Hagel, J. & Vogel, H. J. The structure of the antimicrobial peptide Ac-RRWWRF-NH2 bound to micelles and its interactions with phospholipid bilayers. *J. Pept. Res.* **61**, 219–229 (2003).

91. Chan, D. I., Prenner, E. J. & Vogel, H. J. Tryptophan- and arginine-rich antimicrobial peptides: Structures and mechanisms of action. *Biochim. Biophys. Acta - Biomembr.* **1758**, 1184–1202 (2006).

92. Nguyen, L. T. *et al.* Serum stabilities of short tryptophan- and arginine-rich antimicrobial peptide analogs. *PLoS One* **5**, 1–8 (2010).

93. Knappe, D., Henklein, P., Hoffmann, R. & Hilpert, K. Easy strategy to protect antimicrobial peptides from fast degradation in serum. *Antimicrob. Agents Chemother.* **54**, 4003–4005 (2010).

94. Mekaj, Y. H. The roles of platelets in inflammation, immunity, wound healing and malignancy. *Int. J. Clin. Exp. Med.* **9**, 5347–5358 (2016).

95. Kryczka, J. & Boncela, J. Leukocytes: The Double-Edged Sword in Fibrosis. *Mediators Inflamm.* **2015**, (2015).